

PHYSICS OF THE QUARK-GLUON PLASMA

Berndt Müller

Department of Physics
Duke University
Durham, NC 27708-0305

Abstract

Central nuclear collisions at energies far above 1 GeV/nucleon may provide for conditions, where the transition from highly excited hadronic matter into quark matter or quark-gluon plasma can be probed. Here I review our current understanding of the physical properties of a quark-gluon plasma and review ideas about the nature of, and signals for, the deconfinement transition. I also give a detailed presentation of recent progress in the treatment of the formation of a thermalized state at the parton level.

INTRODUCTION

Overview

After a collision between a ^{32}S nucleus of 6.4 TeV total energy and a heavy target nucleus several hundred charged particles are emitted. No one in his or her right mind would care to study such events, unless there existed a compelling reason for doing so. The current interest in nuclear collisions at very high energies (far above 1 GeV/u in the c.m. system) is fueled by the expectation that a *quark gluon plasma* may be created temporarily in these events¹⁻³. Whereas there is general consensus among theorists that QCD at thermodynamic equilibrium exhibits a phase transition from the normal color-confined phase of hadronic matter with broken chiral symmetry to a deconfined, chirally symmetric phase at sufficiently high energy density, many aspects of this transition are still a matter of debate. Such “details” are, e.g., the order of the phase transition, the precise value of the critical energy density, the nature of experimentally observable signatures of the transition, and how fast thermal equilibrium conditions are established in nuclear collisions over a sufficiently large space-time volume. These questions require much further theoretical and experimental study. Here we are concerned with an up-to-date survey of (mostly) theoretical aspects. More detailed discussions of selected theoretical topics, as well as reviews of experimental results, can be found in other lectures presented at this school.

The “Cosmic” Connection

Perhaps the most compelling reason why we should attempt to study the quark-gluon plasma transition in laboratory experiments is that it must have occurred in the early universe⁴. The history of the thermal evolution of our universe is depicted in Fig. 1. The relation between temperature T and cosmic time t is approximately given by⁵:

$$T_{\text{MeV}} \simeq (5.75 N_f(T))^{1/4} t_{\text{sec}}^{-1/2},$$

where $N_f(T)$ describes the number of particle degrees of freedom that act as effectively massless modes at a given temperature, and the subscripts indicate the units in which T and t are measured. From the present temperature of the cosmic background radiation (2.7 K) we extrapolate back to a temperature of about $2 \times 10^{12} \text{K} \simeq 200 \text{ MeV}$ at about $20 \mu\text{s}$ after the “big bang”. This is the temperature above which, as we will discuss in detail below, hadrons dissolve and their constituent quanta, quarks and gluons, are liberated.

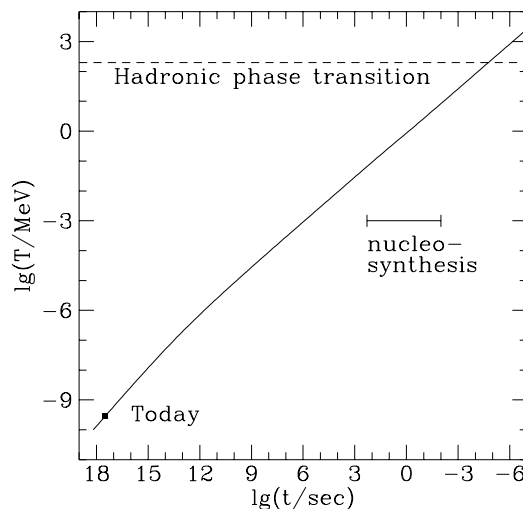


Figure 1. Thermal history of the Universe.

Tracing the history of our universe backward, this is only the first phase transition involving fundamental quantum fields that we encounter. Most likely, more transformations of a similar nature have occurred at even earlier times. If our current ideas of the origin of electroweak symmetry breaking are correct, a phase transition in the Higgs vacuum took place at $t \approx 10^{-11} \text{s}$, when the temperature was around 250 GeV. A similar phase transition at much earlier times ($t \approx 10^{-35} \text{s}$) associated with the “grand” unification of electroweak and strong interactions may have led to exponential inflation of cosmic scales, due to the anti-gravitational pressure exerted by an unstable vacuum state^{6,7}.

Why should we care about events occurring at such unimaginably short moments after the creation of our universe? The reason is that some of the unsolved problems of cosmology are, most likely, associated with events in the era before about 10^{-5}s :

- The observed *baryon number asymmetry* in the universe is probably due to baryogenesis by topologically nontrivial field configurations during the electroweak phase transition.

- The nature of *dark matter* may be associated with properties of the Higgs or the QCD vacuum.
- The near *isotropy of the background radiation*, and the deviations from homogeneity underlying the observed *large-scale structure* of the universe were, according to current thinking, determined during the phase transition causing inflation.

Understanding of the dynamical nature of phase transitions in elementary quantum field theories is thus essential to further progress toward the solution of these puzzles. Since the QCD phase transition is the only one of these that appears accessible to laboratory experiments, we must study it with high priority.

Quark Stars

In addition to events in the very early universe, quark matter may also play a role in the internal structure of collapsed stars. At the high densities reached in the core of neutron stars nucleons may well dissolve into their constituents, forming baryon-rich cold quark matter. This would not lead to greater stability of neutron stars, quite to the contrary: since quark matter would allow for a higher central density of the star at a given total star mass, its formation would actually facilitate collapse to a black hole. Neutron stars with a quark core have a lower value of their upper mass limit, probably somewhere between 1.5 and 2 solar masses⁸. Stars with a quark core would be more compact and hence could sustain higher rotation rates⁹. This observation would be of practical interest, if pulsars with periods in the sub-millisecond range are eventually detected.

The problem with quantitative predictions here is that dense baryon-rich nuclear matter is expected to contain a large strangeness fraction, because the inclusion of strange quarks can lower the Fermi energy. This holds true for baryonic matter as well as quark matter. Unfortunately the equation of state of baryonic matter containing hyperons is poorly known. The scalar coupling strength of Λ -hyperons, which is not well determined experimentally has a large influence on the central density of hyperon-rich neutron stars. This uncertainty can easily mask the formation of a quark matter core⁸. Better understanding of the equation of state of hyperon interactions in dense baryon-rich matter, which can only come from high-energy nuclear collisions, is therefore essential for further progress towards the understanding of neutron star structure.

THE EQUATION OF STATE OF HADRONIC MATTER

There are two approaches that have been widely followed to the problem of the equation of state of strongly interacting matter:

- Consider color-singlet hadrons, i.e. baryons and mesons, only and see how far one gets with taking into account their known interactions and excitation spectra. This approach was pioneered by R. Hagedorn, and later studied by Hagedorn and Rafelski¹⁰, Walecka¹¹, Gasser and Leutwyler¹², and many others.
- Consider the fundamental constituents of hadrons, i.e. quarks and gluons, and study the equation of state on the basis of quantum chromodynamics. This approach, anticipated in pre-QCD days by P. Carruthers¹³, was pioneered by Collins and Perry¹⁴, Baym and Chin¹⁵, McLerran et al.¹⁶ and by Shuryak¹⁷.

Here we will start by examining the approach based on hadrons and their interactions, because its results are important in their own right. Any quark-gluon plasma formed in a nuclear reaction will eventually hadronize and evolve through a

hadron-dominated break-up phase. In addition, potential signatures for quark-gluon plasma formation must always be compared with predictions of a scenario that makes no reference to a phase transition from color-singlet hadrons to deconfined quarks and gluons.

Hot and Dense Hadronic Matter

How far do we get in explaining the equation of state of hadronic matter by considering hadrons alone? Experimental observations of baryon and meson resonances indicate that the mass density of hadronic states grows exponentially,

$$\rho(m) \simeq m^a \exp(m/m_0) \quad (1)$$

as originally postulated by Hagedorn¹⁸. It is now understood that an exponential mass spectrum is the natural consequence of quark confinement, and it is found in even the simplest hadron models that incorporate the confinement concept, such as the string model¹⁹ or the MIT-bag model²⁰. A numerical simulation of the spectrum of excited string modes agrees very nicely with the observed hadron spectrum even at low energies²¹.

Now consider highly excited hadronic matter, characterized by a temperature T . The energy density of excited states is then given by (2.1) integrated over momentum space, i.e.

$$\begin{aligned} n(E) &\simeq \exp(-E/T) \int_0^E dm \rho(m) E \sqrt{E^2 - m^2} \\ &\simeq E^{a+2} \exp \left[-E \left(\frac{1}{T} - \frac{1}{m_0} \right) \right]. \end{aligned} \quad (2)$$

Obviously, $n(E)$ is only integrable as long as the factor in the exponent remains positive, i.e. for $T < T_c \equiv m_0$. From experimental data we know that $m_0 \approx 200$ MeV, i.e. the temperature of a (noninteracting) hadronic resonance gas cannot exceed the Hagedorn temperature $T_c \sim 200$ MeV. Cabibbo and Parisi pointed out in 1975 that the distribution (2) remains integrable at $T = T_c$ when $a < -4$, and then corresponds to a finite energy density $\varepsilon = \int E dE n(E)$ at the critical point²². This is reminiscent of the singular behavior of thermodynamical quantities at a first-order phase transition, and they speculated that it signals the transition to a color-deconfined quark-gluon plasma.

Although Hagedorn has stressed that the inclusion of hadronic resonances effectively accounts for a large part of the interactions among hadrons, not all interactions are taken into account in this simple manner, especially if one neglects the resonance widths. When Hagedorn and Rafelski²³ studied the effect of the finite internal size of hadrons by utilizing the finite excluded volume approximation, they found that the equation of state developed a singularity at finite energy density at a slightly lower critical temperature $T_c < m_0$, independent of other details of the hadronic mass spectrum (2.1). We conclude from all this that hadronic matter as composed of individual color-singlet hadrons ceases to exist at temperatures exceeding $T_c \simeq 150$ -200 MeV.

Medium Modifications of Hadron Structure

It is useful to sharpen the question concerning the influence of interactions on the hadronic equation of state and ask whether hadron masses themselves depend on temperature and density. As this interesting problem has been approached from several different angles, it is quite enlightening to discuss a few of these.

(a) *Sigma-condensate models:*

In these models the nucleon mass M is generated by the coupling to a scalar field σ :

$$\mathcal{L}_N = \bar{\psi}i\gamma \cdot \partial\psi - g\bar{\psi}\psi\sigma, \quad (3)$$

which develops a nonvanishing vacuum expectation value

$$\sigma_0 \equiv \langle 0|\sigma|0\rangle = M/g. \quad (4)$$

However, since the σ -field interacts with hadrons, via an equation of the form

$$(\partial^2 + \mu_\sigma^2)(\sigma - \sigma_0) = -g\langle\bar{\psi}\psi\rangle, \quad (5)$$

its expectation value is shifted in dense nuclear matter according to the equation

$$M^* = g\sigma = M - \frac{g^2}{\mu_\sigma^2}\langle\bar{\psi}\psi\rangle. \quad (6)$$

Here

$$\langle\bar{\psi}\psi\rangle = 4 \int \frac{d^3k}{(2\pi)^3} \frac{M^*}{E(k)}(n(k) + \bar{n}(k)) \quad (7)$$

is the scalar baryon density, $E(k)^2 = k^2 + M^{*2}$, and $n(k), \bar{n}(k)$ denote the momentum space density of baryons and antibaryons, respectively. The numerical evaluation of eq. (2.6) shows that M^* drops rather suddenly to a very small value at $T \simeq 200$ MeV at zero net baryon density ρ^{11} . The decrease with ρ at $T = 0$ is more gradual, already corresponding to $M^*/M \simeq 0.6$ at nuclear matter saturation density ρ_0 . M^* becomes very small at $\rho/\rho_0 \sim 3 - 4$.

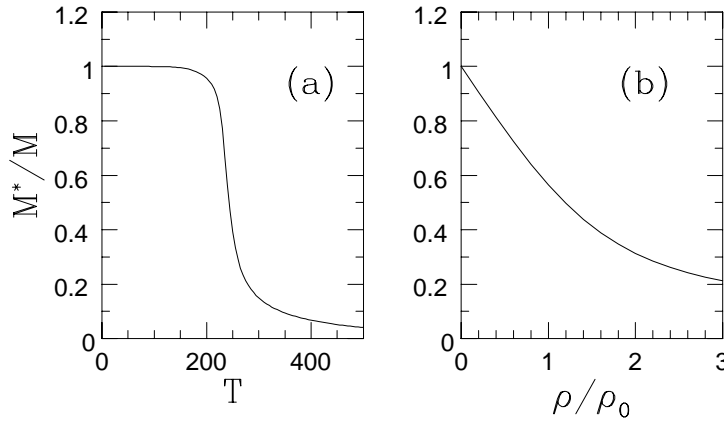


Figure 2. Effective mass of the nucleon in the σ - ω model: (a) as function temperature T at $\rho=0$, (b) as function of the baryon density ρ at $T = 0$.

(b) *Dispersion relations:*

A second method of approach makes use of available data on hadron-hadron scattering via dispersion relations. The propagator of a hadron, say a pion or kaon, in medium is modified due to interactions with other particles. In many cases this interaction is dominated by resonance scattering, schematically illustrated in Figure 3. This is the case, e.g., for pions which interact with other pions from the medium to form a short-lived rho-meson, and with kaons that form a K^* resonance. This also occurs with K^- mesons interacting with nucleons via the Σ^* resonance at 1385 MeV, but *not* with K^+ mesons which have a dominantly nonresonant interaction with nucleons.



Figure 3. Resonance scattering on pions from the medium leads to a medium-dependent mass shift of (a) pions, (b) kaons.

The in-medium propagator of a (pseudo-) scalar meson has the form

$$D(k) = (k^2 - m_i^2 - \Pi_i(k))^{-1} \equiv (k^2 - m_i^*(k)^2)^{-1} \quad (8)$$

where i denotes the meson species and the polarization function $\Pi_i(k)$ can be expressed as the sum of the contributions from interactions with all other hadrons contained in the medium²⁴:

$$\Pi_i(k) = \sum_j \int \frac{d^3p}{(2\pi)^3} \frac{8\pi}{E_p} \frac{1}{\sqrt{s}} f_{ij}(0, s) n_j(p). \quad (9)$$

Here $f_{ij}(0, s)$ is the forward scattering amplitude at energy $s = (p + k)^2$ and $n_j(p)$ denotes the momentum space density of hadrons of species j in the medium. Numerical evaluation of expression (8) for pions and kaons reveals rather small mass shifts $\Delta m_i = m_i^*(\vec{k} = 0) - m_i$ of order 10-30 MeV in baryon-symmetric hadronic matter up to temperatures around 150 MeV, beyond which the approximations entering into (9) become unreliable.

However, it turns out that the effect on kaons in *baryon-rich* matter can be substantial. As shown in Figure 4, the mass shift of kaons at $T = 160$ MeV and baryon density $\rho = 4\rho_0$ is of the order of 100 MeV, being positive for K^+ and negative for K^- . The reason for the opposite behavior is that the interaction of K^- -mesons with nucleons is resonance-dominated and attractive, whereas the interaction of K^+ -mesons is nonresonant and repulsive. An immediate consequence of the different mass shift is that the relative abundance of charged kaons in dense baryon-rich matter is modified²⁵. In fact, the mass shift acts counter to the effect of the nonvanishing baryochemical potential and limits the ratio of abundances K^+/K^- to about 5 at $T \simeq 150$ MeV even for extreme baryon density. Notably this is just the ratio observed in heavy ion collisions at the AGS²⁶. Is this a coincidence? Although kaons in these reactions are probably emitted long after the moment of highest density in the fireball, the K^+/K^- ratio may be determined by the reactions occurring at or before the moment of highest compression. The abundances probably get out of equilibrium and remain frozen as the fireball expands and breaks up rapidly.

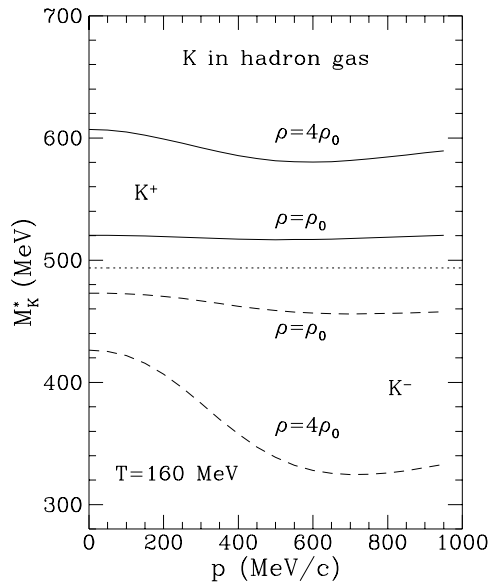


Figure 4. Mass shift of kaons in baryon-rich hadronic matter. The figure shows the medium-dependent change in the energy of positive kaons (solid lines) and negative kaons (dashed lines) as function of momentum for $T = 160$ MeV and twodifferent baryon densities.

(c) *QCD sum rules:*

A third avenue of approach to medium modifications of hadronic properties touches base with the underlying QCD dynamics by identifying the sigma condensate σ_0 with the scalar quark-antiquark condensate $\langle \bar{q}q \rangle$ in QCD. This permits one to advance the argument²⁷ that *all* hadron masses should be modified in the *same* way, according to

$$\frac{m_i^*}{m_i} = \frac{\langle \text{med} | \bar{q}q | \text{med} \rangle}{\langle 0 | \bar{q}q | 0 \rangle}. \quad (10)$$

A qualitative estimate of the change in hadron masses can then be obtained from any estimate of the scalar quark density in the medium, as compared with the vacuum condensate²⁸

$$\langle 0 | \bar{q}q | 0 \rangle = -(225 \pm 25 \text{MeV})^3. \quad (11)$$

A simple way to estimate the medium contribution to $\langle \bar{q}q \rangle$ is to calculate the scalar quark density contained in the thermal pions

$$\delta \langle \bar{q}q \rangle_\pi = 3 \int \frac{d^3k}{(2\pi)^3} \langle \pi(k) | \bar{q}q | \pi(k) \rangle n_\pi(k), \quad (12a)$$

or, for baryon-rich matter, in the nucleons

$$\delta \langle \bar{q}q \rangle_N \simeq 4 \int \frac{d^3k}{(2\pi)^3} \langle N(k) | \bar{q}q | N(k) \rangle n_N(k). \quad (12b)$$

Eq. (12a) may be conveniently evaluated in the framework of chiral perturbation theory¹². Results are shown in Figure 5a. More model-independent estimates for (12a,b) can be obtained by the so-called QCD sum-rule approach²⁹⁻³¹. Figure 5b shows the predictions of this technique for the medium modifications of the condensates of light quarks, strange quarks and gluons in the QCD vacuum as function of

baryon density (at $T = 0$). Obviously, the condensate of light quarks is most strongly affected in both approaches, indicating a dramatic change in hadron structure at $T \approx 200$ MeV or $\rho \simeq 4\rho_0$.

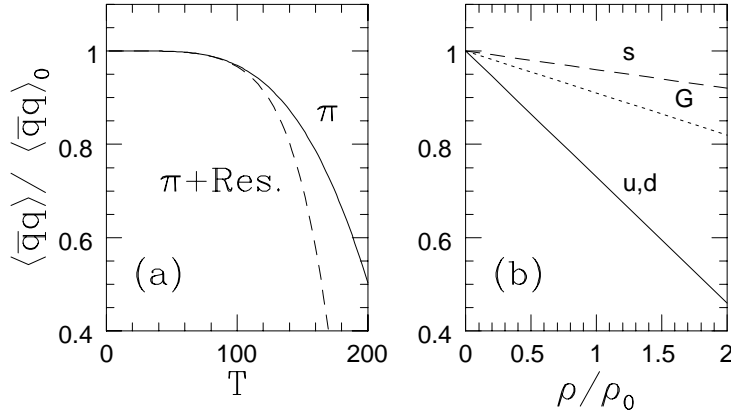


Figure 5. Medium modification of QCD condensates. (a) Change of the quark condensate in a pion gas as function of temperature¹². (b) Dependence of the condensates of light quarks, gluons and strange quarks as functions of the baryon density³¹.

Overall, the agreement between the predictions of the different approaches agree remarkably well, reinforcing faith in their accuracy. In general, one finds that hadron structure is much less disturbed by a baryon symmetric medium of finite temperature than by a medium with finite net baryon density. The right place to look for medium effects on hadron structure is therefore in relativistic nuclear collisions involving a large degree of baryon stopping, such as the Brookhaven AGS — especially with the ^{197}Au beam — or possibly the CERN-SPS in Pb+Pb collisions. In the case of matter depleted of baryons the medium effects set in so late that it will be very difficult to disentangle them from the quark-gluon plasma phase transition.

QUARK-GLUON PLASMA

The theory of the equation of state of quark matter is conceptually much simpler, because it is directly based on the fundamental QCD Lagrangian

$$\mathcal{L}_{\text{QCD}} = -\frac{1}{4} \sum_a F_{\mu\nu}^a F^{a\mu\nu} + \sum_{f=1}^{N_f} \bar{\psi} (i\gamma^\mu \partial_\mu - g\gamma^\mu A_\mu^a \frac{\lambda^a}{2} - m_f) \psi \quad (13)$$

where the subscript f denotes the various quark flavors u, d, s, c , etc., and the non-linear glue field strength is given by

$$F_{\mu\nu}^a = \partial_\mu A_\nu^a - \partial_\nu A_\mu^a + gf_{abc} A_\mu^b A_\nu^c. \quad (14)$$

QCD predicts a weakening of the quark-quark interaction at short distances (or high momenta Q^2), because the one-loop series for the gluon propagator yields a running coupling constant

$$g^2(Q^2) = \frac{16\pi^2}{(11 - \frac{2}{3}N_f) \ln(Q^2/\Lambda^2)} \xrightarrow{Q^2 \rightarrow \infty} 0. \quad (15)$$

The QCD scale parameter is now quite well determined³² to be $\Lambda \simeq 150$ MeV. The vanishing of the QCD coupling constant at short distances, called “asymptotic freedom”, has often been taken to imply that interactions among quarks and gluons are negligible in the limit of high temperature or high density. As we shall see below this is not the whole truth, because long-wavelength modes continue to have an important influence on the properties of the quark-gluon plasma.

Equation of State of Quark Matter

So let us first suppose that interactions among quarks and gluons are negligible at high energy density and see what we get. At temperature T and quark chemical potential μ (one-third of the baryochemical potential $\mu_B = 3\mu$), the energy density of free gluons, quarks and antiquarks is (a detailed derivation can be found in ref. 1):

$$\varepsilon_g = 16 \frac{\pi^2}{30} T^4. \quad (16a)$$

$$\varepsilon_q + \varepsilon_{\bar{q}} = 6N_f \left(\frac{7\pi^2}{120} T^4 + \frac{1}{4} \mu^2 T^2 + \frac{1}{8\pi^2} \mu^4 \right). \quad (16b)$$

Since we have neglected the quark mass, we inserted a factor N_f counting the number of quark flavors active at a given temperature (essentially those with $m_f \leq T$). Clearly $N_f \geq 2$ at all relevant temperatures, and $N_f = 3$ in the range $200 \text{ MeV} \ll T < 1 \text{ GeV}$ where strange quarks can be considered as light, as well. The other thermodynamical quantities of interest, i.e. pressure P , entropy density s , and baryon number density ρ_B , are easily obtained from eqs. (16):

$$P = \frac{1}{3} \varepsilon, \quad s = \left(\frac{\partial P}{\partial T} \right)_\mu, \quad \rho_B = \frac{1}{3} \left(\frac{\partial P}{\partial \mu} \right)_T. \quad (17)$$

Note that the simple relation between ε and P holds only as long as all particles are considered massless. The general relation is

$$\varepsilon = T \left(\frac{\partial P}{\partial T} \right)_\mu + \mu \left(\frac{\partial P}{\partial \mu} \right)_T - P \equiv Ts + \mu_B \rho_B - P. \quad (18)$$

In order to find the location of the phase transition toward hadronic matter we have to incorporate the breaking of scale invariance provided by QCD interactions. The simplest way of achieving this is by invoking the argument associated with the MIT-bag model: Free quarks and gluons can only propagate where the complex structure of the real QCD vacuum has been destroyed. The vacuum realignment costs a certain amount of energy per unit volume, expressed by the MIT-bag constant $\varepsilon_0 = B \simeq (150\text{-}200 \text{ MeV})^4$, and the “wrong” vacuum is endowed with a negative pressure $P_0 = -B$. The relation $\varepsilon_0 = -P_0$ is mandated by the Lorentz invariance of the vacuum state. The negative sign is easily understood as signal of the instability of the wrong vacuum state which collapses if not supported by the pressure provided by free partons propagating in the volume filled with it. The equation of state of the quark-gluon plasma then takes the simple form

$$\varepsilon = \varepsilon_g(T, \mu) + \varepsilon_q(T, \mu) + \varepsilon_{\bar{q}}(T, \mu) + B; \quad (19a)$$

$$P = P_g(T, \mu) + P_q(T, \mu) + P_{\bar{q}}(T, \mu) - B. \quad (19b)$$

A lower limit of stability of the plasma state is obtained by setting $P = 0$. This yields the stability line in the T - μ plane shown in Figure 6. Of course, the plasma phase becomes unstable against formation of a gas of color-singlet hadrons even earlier, when its pressure equals that of a hadron gas at the same temperature T and chemical potential μ .

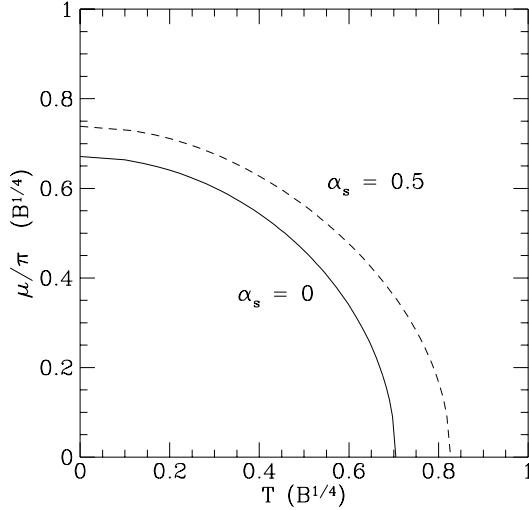


Figure 6. Stability line of the quark-gluon plasma in the T - μ plane for two values of the strong coupling constant. The lines indicate where the pressure of a gas of quarks and gluons vanishes. The quark-gluon plasma is unstable in the lower left region of the figure.

In order to explore this aspect further, let us restrict ourselves to the baryon-free case $\mu = 0$, and explore the coexistence between the quark-gluon plasma phase given by eq. (19a) and hadronic matter, represented by a gas of massless, noninteracting pions:

$$\varepsilon_\pi = 3 \frac{\pi^2}{30} T^4, \quad P_\pi = \frac{1}{3} \varepsilon_\pi. \quad (20)$$

ε , P , ε_π and P_π are shown as functions of T in Figure 7.

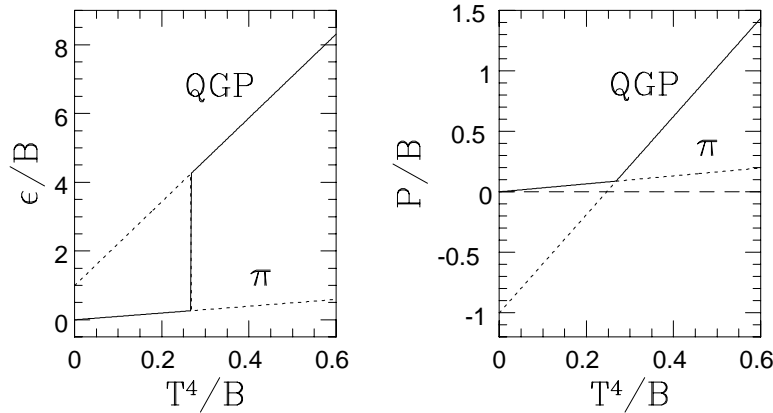


Figure 7. Energy density and pressure of a pion gas and a free quark-gluon gas as function of temperature. A first-order phase transition occurs where the pressure of the two phases is equal. The solid line indicates the stable phase.

Thermodynamical phase stability requires that the phase with the larger pressure dominates, and phase equilibrium is achieved when $P(T_c) = P_\pi(T_c)$. As Figure 7b shows, one finds $T_c \simeq 0.75B^{\frac{1}{4}} \simeq 150$ MeV with $B \simeq (200 \text{ MeV})^4$ in this model. Due to the vacuum rearrangement energy B , the energy density between the two phases differs greatly at this point, by the amount $\Delta\varepsilon_c \simeq 4B \simeq 0.8 \text{ GeV}/\text{fm}^3$. This simple model obviously predicts a first-order phase transition between the pion gas and quark-gluon plasma with a large latent heat $\Delta\varepsilon_c$.

Of course, our model is grossly oversimplified because, as we saw earlier, other hadron masses begin to decrease substantially around $T \simeq 150$ MeV, leading to an increase in the energy density of the hadronic phase. In parallel, interaction between quarks and gluons cause a reduction in the energy density and pressure of the plasma phase. In first-order perturbation theory, the modification of the plasma equation of state is (for $N_f = 2$):

$$\begin{aligned} \varepsilon = & \left(1 - \frac{15}{4\pi}\alpha_s\right) \frac{8\pi^2}{15} T^4 + \left(1 - \frac{50}{21\pi}\alpha_s\right) \frac{7\pi^2}{10} T^4 + \\ & + \left(1 - \frac{2}{\pi}\alpha_s\right) \frac{3}{\pi^2} \mu^2 \left(\pi^2 T^2 + \frac{1}{2}\mu^2\right) + B \end{aligned} \quad (21)$$

yielding a reduction by about a factor 2 when $\alpha_s = 0.5$.

More reliable predictions concerning this phase transition can at present only be obtained by numerical simulations of the QCD equation of state on a discretized volume of space-time, usually referred to as *lattice gauge theory*. In this approach³³ one approximately calculates the partition function for a discretized version of the QCD Lagrangian (13) by Monte-Carlo methods. In principle, this technique should accurately describe the quark-gluon plasma as well as the hadronic phase but, in practice, its accuracy especially at low temperature is severely limited by finite size effects and other technical difficulties. Where the numerical results are most reliable, i.e. for the pure gluon theory without dynamical quarks, the calculations predict a sudden jump in the energy density at a certain temperature while the pressure rises more gradually, as shown in Figure 8.

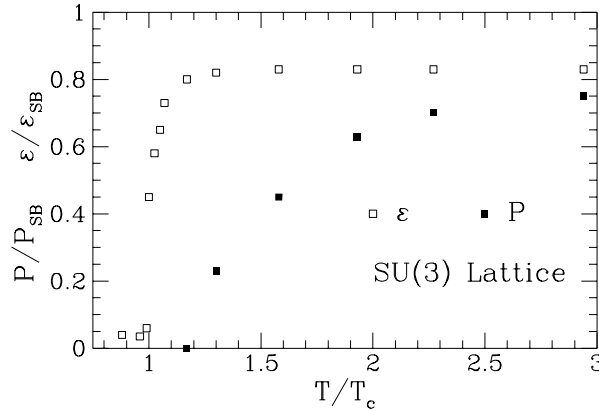


Figure 8. Energy density ε and pressure P of pure glue matter as calculated by simulations of SU(3) lattice gauge theory⁵⁶. ε and P are plotted relative to the Stefan-Boltzmann limit, eq. (16a).

When dynamical quarks are added, the picture becomes less clear for two reasons. One is that the calculations involving fermion fields on the lattice are much more

time consuming, and hence the numerical results are less statistically meaningful and reliable. Moreover, the definition of quark confinement becomes rather fuzzy in the presence of light quarks, because the color flux tube between two heavy quarks can break by creation of a light quark pair: $Q\bar{Q} \rightarrow (Q\bar{q})(q\bar{Q})$. E.g., highly excited states of charmonium can break up into a pair of D-mesons. Thus, in the calculations the $Q\bar{Q}$ potential does not rise linearly with distance, but is effectively screened.

For massless dynamical quarks there exists a new order parameter, the quark-antiquark condensate $\langle 0|\bar{q}q|0\rangle$ in the vacuum. When it assumes a nonzero value, chiral symmetry is spontaneously broken, as can be seen as follows: The scalar quark density has the chiral decomposition $\bar{q}q = \bar{q}_L q_R + \bar{q}_R q_L$, hence the broken vacuum state contains pairs of quarks of opposite chirality. A left-handed quark, say, can therefore annihilate on a left-handed antiquark in the vacuum condensate, liberating its right-handed partner. This process is perceived as change of chirality of a free quark, which is exactly the same result as that of a nonvanishing quark mass. However, in reality the mass of the light quarks u, d is nonzero, and the chirality of a light quark is never exactly conserved.

All one can do, therefore, is to look for sudden changes in the distance at which color forces are screened, or in the quark condensate. If these are discontinuous, one deals with a phase transition, otherwise with a possibly rapid, but continuous change of internal structure as it occurs, e.g., in the transformation of an atomic gas into an electromagnetic plasma. The identification of the nature of the phase change is complicated by finite size effects. The best published results, by the Columbia group³⁴, for a $16^3 \times 4$ lattice indicate a surprisingly strong dependence of the phase diagram on the magnitude of the strange quark mass. For the physical mass $m_s \simeq 150$ MeV there seems to be no discontinuity, but only a rapid change in the energy density over a small temperature range (about 10 MeV). However, it is probably premature to consider this as the final word.

Intermezzo: Astrophysical Implications

We will return to the results of lattice gauge theory in a moment, but let us pause briefly to study some astrophysical implications of a hadron-quark-gluon phase transition. If it is indeed of first order, as the results discussed so far suggest, both phases can coexist over a certain range of temperatures. In particular, the quark-gluon phase can exist in a supercooled state between the critical temperature T_c , where its pressure falls below that of an isothermal hadron gas, and the temperature T , where its pressure becomes negative signaling intrinsic instability of this phase (see Figure 7b). The conversion of the metastable quark-gluon phase into hadrons then proceeds by the formation and subsequent growth of bubbles of hadronic gas imbedded in the plasma. The dynamics of bubble formation is governed by the free energy difference as a function of bubble radius R :

$$\Delta E(R) = -\Delta P \frac{4\pi}{3} R^3 + \sigma 4\pi R^2 + aR + \dots, \quad (22a)$$

where $\Delta P > 0$ is the difference in pressure between the two phases, σ is the surface tension of the interface, and a is a coefficient related to the Casimir energy of the bubble configuration. The function $\Delta E(R)$ is schematically depicted in Figure 9a. The notable feature here is the fact that bubble formation is thermodynamically discouraged for small bubbles. Only when a bubble grows to a radius $R > R_c$, where R_c denotes the location of the maximum $\Delta E_c \simeq 2\sigma/\Delta P$, due to some thermal fluctuation will it continue to grow on its own. As the probability of forming such a *critical droplet*³⁵ is obviously hindered by a factor $\exp(-\Delta E_c/T)$, the suppression depends

sensitively on the size of the interface energy σ . Its value has recently been calculated in the framework of QCD-related models³⁶ as well as by lattice simulations³⁷. All results indicate that the surface tension should be small:

$$\sigma \simeq 20\text{-}50 \text{ MeV/fm}^2, \quad (23)$$

implying that it is probably difficult to supercool a quark-gluon plasma for a considerable time (see ref. 38 for a recent discussion).

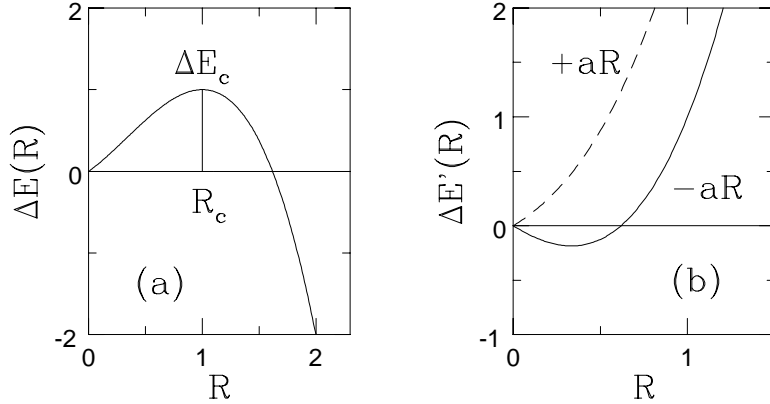


Figure 9. Energy of a hadronic bubble in the quark-gluon plasma versus its radius: (a) for $T < T_c$, (b) for $T > T_c$. R_c in (a) indicates the critical droplet. The solid curve in (b) predicts the “Swiss cheese” instability of a quark-gluon plasma against formation of small inhomogeneities.

On the other hand the small surface tension raises the importance of the next term in the series (22a), which is linear in the bubble radius R . That may have a dramatic effect when we consider the opposite case, namely, superheated hadronic matter droplets forming inside a large quark-gluon plasma bubble. This is precisely the situation one hopes to find right after a highly energetic nuclear collision. When we now ask about the stability of the plasma, we must consider the reverse situation described by a droplet energy obtained from (22a) by altering the signs of all terms with an odd power of R (see solid curve in Figure 9b):

$$\Delta E'(R) = \Delta P \frac{4\pi}{3} R^3 + \sigma 4\pi R^2 - aR + \dots \quad (22b)$$

The change in sign of the linear (as well as the cubic) term was pointed out by Lana and Svetitsky³⁹ who went on to study its possible consequences. Since the linear term dominates $\Delta E'(R) < 0$ for small R , and it is favorable to break up the plasma by forming small droplets of superheated hadronic matter inside. This has been termed the “Swiss cheese instability” of the quark-gluon plasma. More detailed studies show the hadronic droplets to be unstable against deformations, pointing to the possibility that the plasma phase may be characterized by a complex structure of inhomogeneities in the region of phase coexistence. There is preliminary support for this exotic picture from lattice simulations⁴⁰.

Perhaps the most important effect caused by coexistence of the two phases is due to the difference between the baryon densities in them at equilibrium⁴¹. As discussed above, the baryon density in the quark-gluon phase at given temperature T and baryochemical potential μ_B is (using eqs. 21, 17):

$$\rho_B^{(Q)} \simeq \frac{2}{3} \mu_B \left(T^2 + \frac{1}{9\pi^2} \mu_B^2 \right), \quad (24)$$

whereas the net baryon density in the hadronic phase (counting only nucleons, not excited baryon resonances):

$$\rho_B^{(H)} \simeq 8 \frac{\mu_B}{T} \left(\frac{m_N T}{2\pi} \right)^{3/2} e^{-m_N/T}, \quad (25)$$

where m_N is the nucleon mass. The ratio $\rho_B^{(Q)}/\rho_B^{(H)}$ is very sensitive to the precise value of the critical temperature T_c ; but generally one finds $\rho_B^{(Q)} \gg \rho_B^{(H)}$, as illustrated in Figure 10.

Consequently, if the transition proceeds at or near chemical equilibrium, baryons become enriched in the quark-gluon plasma phase. For some time it was speculated that this effect could result in local fluctuations of the proton-neutron ratio in the early universe that were large enough to influence the course of nucleosynthesis. The argument goes roughly as follows: Neutrons will quickly diffuse away from a local surge in the baryon density, leaving behind a region of abnormally large proton-neutron ratio. Nucleosynthesis there will result in a reduced number of neutron-rich isotopes, such as ${}^4\text{He}$ and ${}^7\text{Li}$. However, if the size of the region of anomalous baryon concentration is too small (less than about 20 m) neutrons can diffuse back during the era of nucleosynthesis and even things out. For the small value of the interface tension σ , eq. (23), the effect of local inhomogeneities in the baryon density is probably negligible^{43,44}.

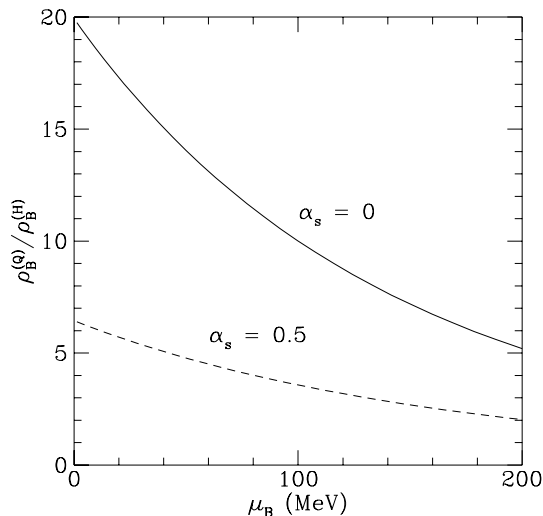


Figure 10. Ratio of the baryon densities of the quark-gluon plasma and a hadronic gas at the coexistence line as function of the baryochemical potential μ_B . Conditions in the early universe correspond to the line $\mu_B=0$.

In relativistic heavy ion collisions, the most important result of the concentration of baryons in the quark matter phase may be that it is accompanied by an enrichment with *strange quarks* (as opposed to strange antiquarks). The interest in such a mechanism derives from speculations that quark matter droplets with a high strangeness content (so-called *strangelets*) might be stable or metastable^{45,41}, because a large fraction of strange quarks allows to construct electrically almost neutral nuclei with large baryon number without raising the proton-neutron asymmetry. As Liu and Shaw⁴⁶, as well as Greiner, Koch and Stöcker⁴⁷ showed, the quark matter—hadron gas phase

transition effectively acts as a distillation process for strange quarks, if there is a net baryon surplus⁴⁸. Several experiments at Brookhaven (AGS) and CERN (SPS) are searching, or preparing to search, for strangelets produced in nuclear collisions⁴⁹. Their existence would have far-reaching technological implications⁵⁰.

INTERACTING QUARK-GLUON PLASMA

Let us return now to our main theme, i.e. the physical properties of a quark-gluon plasma. So far, we have neglected interactions among quarks and gluons in the deconfined phase, except in eq. (21), where we included the contributions of one-loop diagrams to the energy density and pressure of a quark gluon gas:

$$\begin{aligned} \varepsilon^{(1)} = 3P^{(1)} = & \left(1 - \frac{15}{4\pi}\alpha_s\right) \frac{8\pi^2}{15}T^4 + \left(1 - \frac{50}{21\pi}\alpha_s\right) \frac{7\pi^2}{10}T^4 + \\ & + \left(1 - \frac{2}{\pi^2}\alpha_s\right) \frac{3}{\pi^2}\mu^2 \left(\pi^2T^2 + \frac{1}{2}\mu^2\right), \end{aligned} \quad (26)$$

where we have omitted the vacuum energy B, because it is a non-perturbative contribution. Graphically, eq. (26) corresponds to the diagrams

$$\text{---} + \text{---} + \text{---} + \text{---} \quad (27)$$

where dashed lines denote gluons, and straight lines denote quarks. As (26) shows, we still have $P = \frac{1}{3}\varepsilon$. This changes in the next order, because the two-loop contribution to the gluon energy density is found to diverge! The physical reason for this divergence is that gluon and quark degrees of freedom develop an effective mass, which leads to screening of long-range color-electric forces. Technically, the screening mass is obtained by summing an infinite chain of one-loop insertions in the gluon propagator

$$\text{---} + \text{---} + \text{---} + \dots \quad (28)$$

The contribution of all diagrams except the first two (which are already included in (26)) can be summed analytically and yields a contribution to the gluon energy of order $\alpha^{3/2}$ with a rather large coefficient⁵¹.

The QCD Plasmon

We can obtain more insight into the properties of the interacting quark-gluon plasma by looking at the gluon propagator, represented graphically in (28), itself. Because of gauge invariance, $k^\mu D_{\mu\nu}(k) = 0$, it can be decomposed into a longitudinal and a transverse part, which are scalar functions of the variables $\omega = k^0$ and $k = |\mathbf{k}|$. These are most conveniently written in a form borrowed from electrodynamics of continuous media:

$$D_L(\omega, k) = \frac{1}{\varepsilon_L(\omega, k)k^2}, \quad (29a)$$

$$D_T(\omega, k) = \frac{1}{\varepsilon_T(\omega, k)\omega^2 - k^2}, \quad (29b)$$

where the color-dielectric functions are given by⁵²:

$$\varepsilon_L(\omega, k) = 1 + \frac{g^2 T^2}{k^2} \left[1 - \frac{\omega}{2k} \ln \left(\frac{\omega + k}{\omega - k} \right) \right]; \quad (30a)$$

$$\varepsilon_T(\omega, k) = 1 - \frac{g^2 T^2}{2k^2} \left[1 - \left(1 - \frac{k^2}{\omega^2} \right) \frac{\omega}{2k} \ln \left(\frac{\omega + k}{\omega - k} \right) \right]. \quad (30b)$$

Several things are noteworthy about eqs. (29, 30). First they imply that static longitudinal color fields are screened:

$$D_L(0, k) = \frac{1}{\varepsilon_L(0, k)k^2} = \frac{1}{k^2 + g^2 T^2} = \frac{1}{k^2 + \lambda_D^{-2}}. \quad (31a)$$

The Debye length obviously is $\lambda_D = (gT)^{-1}$. On the other hand, eqs. (29b,30b) show that static transverse (magnetic) color fields remain unscreened at this level of approximation:

$$D_T(0, k) = -\frac{1}{k^2}. \quad (31b)$$

The static magnetic screening length is of higher order in the coupling constant; lattice gauge calculations⁵² have shown that $\lambda_M^{-1} = Cg^2 T$.

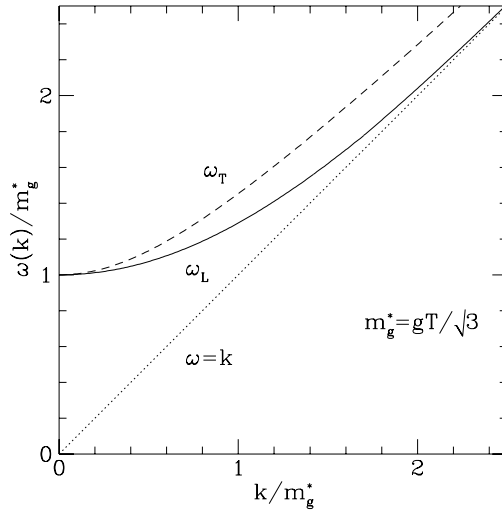


Figure 11. Gluon dispersion relation in the perturbative quark-gluon plasma. All quantities are measured in units of the effective gluon mass $m_g^* = gT/\sqrt{3}$. Solid line: longitudinal plasmon mode; dashed line: transverse collective gluon mode.

For a finite frequency ω the in-medium propagators (29) have poles corresponding to propagating, collective modes of the glue field. The dispersion relation for the longitudinal mode:

$$\varepsilon_L(\omega, k) = 0, \quad (32a)$$

called the *plasmon*, has no counterpart outside the medium. The analogous relation for the transverse mode:

$$\varepsilon_T(\omega, k) = k^2/\omega^2 \quad (32b)$$

describes the effects of the medium on the free gluon. The behavior of both modes is remarkably similar. For $k \rightarrow 0$ they yield an effective gluon/plasmon mass

$$\omega_L, \omega_T \xrightarrow{k \rightarrow 0} m_g^* = \frac{1}{\sqrt{3}} gT, \quad (33)$$

whereas for large momenta ($k \rightarrow \infty$) one finds

$$\omega_L(k) \rightarrow k, \quad \omega_T(k) \rightarrow \sqrt{k^2 + \frac{1}{2}g^2T^2}. \quad (34)$$

The full dispersion relations are shown in Figure 11.

For plasma conditions realistically attainable in nuclear collisions ($T \simeq 250$ MeV, $g = \sqrt{4\pi\alpha_s} \simeq 2$) the effective gluon mass is $m_g^* \simeq 300$ MeV. We must conclude, therefore, that the notion of almost free gluons (and quarks) in the high-temperature phase of QCD is quite far from the truth. Certainly, one has $m_g^* \ll T$ when $g \ll 1$, but this condition is *never* really satisfied in QCD, because $g \simeq \frac{1}{2}$ even at the Planck scale (10^{19} GeV), and $g < 1$ only at energies above 100 GeV. Let us discuss some consequences of these results:

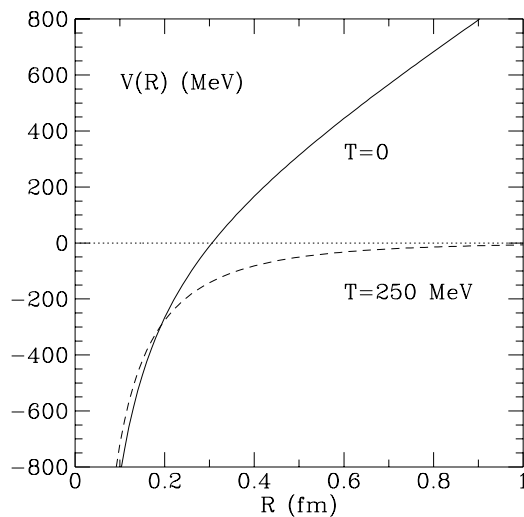


Figure 12. Effective quark-antiquark potential in QCD. Solid line: confining potential of a free $Q\bar{Q}$ pair; dashed line: screened potential, eq. (35), of a $Q\bar{Q}$ pair imbedded in the quark-gluon plasma.

- (1) The potential between two static color charges, such as two heavy quarks, is screened in the quark-gluon plasma phase. The Fourier transform of eq. (31a) yields the potential

$$V_{Q\bar{Q}}(r) \simeq \frac{1}{r} e^{-r/\lambda_D} \quad (35)$$

with screening length $\lambda_D \simeq 0.4$ fm at $T = 250$ MeV. This screened potential is compared in Figure 12 with the confining potential between a free quark-antiquark pair. This screening of long-range color forces is, of course, the origin of quark deconfinement in the high-temperature phase. An important consequence, to be discussed later in the section on plasma signatures, is the disappearance of the bound states of a charmed quark pair ($c\bar{c}$) in the quark-gluon plasma⁵⁴.

- (2) The color screening at large distances cures most infrared divergences in scattering processes between quarks and gluons. A self-consistent scheme implementing this mechanism has been devised by Braaten and Pisarski⁵⁵. It involves the resummation of gluon loops involving gluons with momenta of order gT and has been shown to be gauge invariant when also vertex corrections are taken into account.
- (3) The finite effective gluon mass m_g^* leads to the suppression of long-wavelength gluon modes with $k \leq gT$ in the quark-gluon plasma. As a result, the relation $P = \frac{1}{3}\varepsilon$ is violated and the pressure is reduced. We now have two mechanisms that can be responsible for $P < \frac{1}{3}\varepsilon$: an effective gluon mass m_g^* and a nonvanishing vacuum energy B . A fit to recent SU(3) lattice gauge theory results⁵⁶ with m_g^* and B taken as free parameters shows that probably both mechanisms are at work⁵⁷ (see Figure 13).

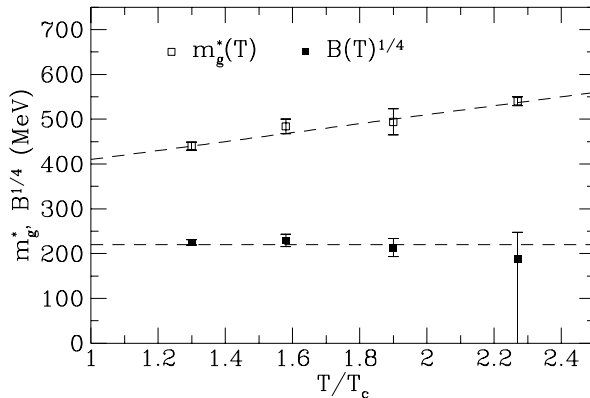


Figure 13. Effective mass m_g^* and vacuum energy density B as function of temperature (lower part) as deduced⁵⁷ from results of lattice gauge theory simulations⁵⁶ for the energy density ε and pressure P of a gluon gas (see Figure 8).

Properties of the Quark-Gluon Plasma

(a) Thermalization:

For those of us interested in the detection of a quark-gluon plasma in nuclear collisions it is imperative to know something about its rate of thermalization. Does it thermalize sufficiently fast, so that a thermodynamical description makes sense? In the picture based on quasi-free quarks and gluons moving through the plasma, thermalization proceeds mainly via two-body collisions, where the color force between the colliding particles is screened, as illustrated in Figure 14. The technically easiest way of looking at this is to consider the quark (gluon) *damping rate* γ , i.e. the imaginary part of the quark (gluon) self energy. For quarks and gluons of typical thermal momenta ($p \simeq T$) one finds with the help of the techniques discussed in the previous section⁵⁵

$$\gamma_q = -\frac{1}{4p} \text{Im}[\text{Tr}(\gamma \cdot p \Sigma(p))] \simeq \frac{2}{3} \alpha_s T \left(1 + \ln \frac{1}{\alpha_s}\right), \quad (36a)$$

$$\gamma_g = -\text{Im}[\omega_T(p)] \simeq \frac{9}{4} \gamma_q, \quad (36b)$$

where the factor $\frac{9}{4}$ reflects the ratio of the quadratic Casimir invariants C_2 of the octet and triplet representations of color-SU(3). Gluons simply have a higher color charge than quarks ($C_2 = 3$ versus $C_2 = \frac{4}{3}$) and therefore scatter more often.

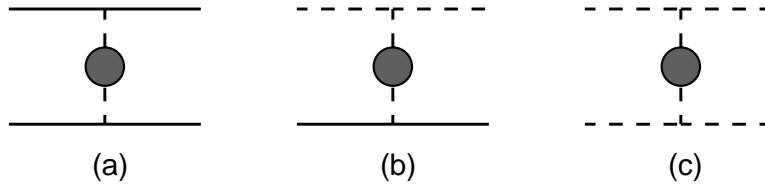


Figure 14. QCD diagrams describing scattering processes contributing to thermalization of the quark-gluon plasma.

One can argue that a better way to look at thermalization is to consider the rate of momentum transfer between particles, i.e. weighting the scattering diagrams of Figure 14 by $\sin^2 \theta$, where θ is the scattering angle. Here one finds⁵⁸:

$$\Gamma_q^{(\text{tr})} \simeq 2.3\alpha_s^2 T \ln \frac{1}{\alpha_s}; \quad \Gamma_g^{(\text{tr})} \simeq 3\Gamma_q^{(\text{tr})}. \quad (37)$$

The *transport rate* $\Gamma^{(\text{tr})}$ is closely related to the shear viscosity of the quark gluon plasma. Both approaches yield quite similar numbers for values of the strong coupling constant in the range $\alpha_s = 0.2-0.5$. The characteristic equilibration time, as defined as the inverse of the rates γ_i or Γ_i are:

$$\tau_g \simeq 1 \text{ fm}/c, \quad \tau_q \simeq 3 \text{ fm}/c, \quad (38)$$

i.e. gluons thermalize about several times faster than quarks⁵⁹. Initially, therefore, probably a rather pure glue plasma is formed in heavy ion collisions, which then gradually evolves into a chemically equilibrated quark-gluon plasma. We shall later return to this point in the context of our discussion of microscopic models of relativistic nuclear collisions, but it is worthwhile to point out one consequence: During its hottest phase the QCD plasma is mainly composed of gluons, which are not accessible to electromagnetic probes, such as lepton pairs and photons. The gluon plasma can only be probed by strongly interacting signals, such as charmed quarks or jets.

(b) Energy loss of a fast parton:

One possible way of probing the color structure of QCD matter is by the energy loss of a fast parton (quark or gluon). The mechanisms are similar to those responsible for the electromagnetic energy loss of a fast charged particle in matter, i.e. energy may be lost either by excitation of the penetrated medium or by radiation. Although radiation is a very efficient energy loss mechanism for relativistic particles, it is strongly suppressed in a dense medium by the Landau-Pomeranchuk effect⁶⁰. In the case of QCD this effect has recently been analyzed comprehensively⁶¹, and the suppression of soft radiation is now firmly established. This limits the radiative energy loss to about 1 GeV/fm. Excitational energy loss proceeds via collisions with quarks and gluons from the plasma. Here again color screening plays an essential role, reducing the rate of energy loss to about 0.3 GeV/fm for a fast quark^{62,63}.

Entropy production

The correspondence principle asserts that highly excited states of a quantum system usually exhibit quasi-classical behavior. Similarly, the high-temperature limit of a quantum system is quasi-classical, since thermal fluctuations dominate over quantum fluctuations.* Since the quark-gluon plasma is the high-temperature phase of QCD, one may ask whether classical, thermal QCD can yield useful results. In view of the remark made in the footnote, most predictions of classical thermal QCD will be cut-off dependent and therefore not completely reliable, except possibly for those quantities that do not involve Planck's constant \hbar . A simple dimensional analysis reveals that the combination $g^2 T$ does not contain factors of \hbar , and therefore one may suspect that the thermalization rate γ_g , eq. (36b), can be obtained by classical considerations. This permits an entirely different, nonperturbative determination of the thermalization rate of gluonic matter by simulation of the dynamics of SU(3) gauge theory in real time on a lattice.

The approach to thermal equilibrium in a classical dynamical system is governed by the rate of entropy production. More precisely, thermodynamic (ensemble) averages can be applied to an isolated classical system, if they coincide with the long-time averages, e.g. of a quantity $A(t)$:

$$\frac{1}{T} \int_0^T dt A(t) \xrightarrow{T \rightarrow \infty} \langle A \rangle_{\text{ensemble}}; \quad (39)$$

such systems are called *ergodic*. It was shown in the important work of Krylov, Kolmogorov, and others⁶⁴ that ergodicity is really of practical use only when the system exhibits the property of *mixing*, meaning that the equality (39) is approached uniformly throughout almost the entire phase space at an exponential rate. This condition, in turn, is satisfied if classical trajectories $\mathbf{x}(t)$ are *unstable* against small fluctuations almost everywhere in phase space. Such systems are also called *strongly chaotic*.

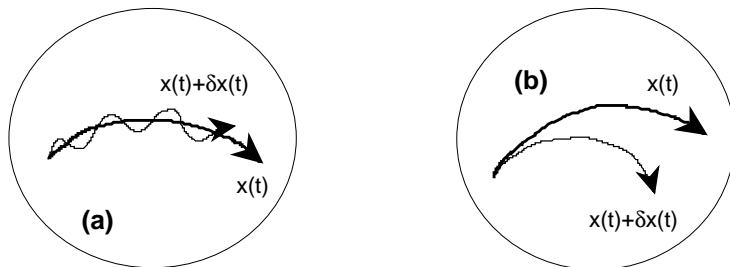


Figure 15. (a) Stable phase space trajectory; (b) unstable trajectory.

Consider two neighboring trajectories, i.e. solutions of the classical equations of motion, $\mathbf{x}(t)$ and $\mathbf{x}'(t) = \mathbf{x}(t) + \delta\mathbf{x}(t)$. The trajectory is *unstable*, if the norm of an infinitesimal derivation grows exponentially with time

$$|\delta\mathbf{x}(t)| \xrightarrow{t \rightarrow \infty} D_0 \exp(\lambda t), \quad \lambda > 0, \quad (40)$$

* As is well-known from the case of electromagnetic black-body radiation, the classical limit is only reached for long-wavelength modes, but not for modes with wavelength $\lambda \ll \hbar/T$. The quasi-classical description therefore requires an ultraviolet cut-off, eliminating these modes.

as illustrated in Figure 15. λ is called a *Lyapunov exponent*. In general, chaotic systems possess several positive Lyapunov exponents, depending on the direction of the initial fluctuation $\delta\mathbf{x}(0)$, but usually the *maximal* Lyapunov exponent λ_0 dominates in eq. (40) for any arbitrarily chosen $\delta\mathbf{x}(0)$.

We are now ready to discuss entropy growth. For a classical system, entropy is defined in terms of the volume in phase space covered by an ensemble of identical systems:*

$$S = \ln(\Delta\Gamma) + \text{const.} \quad (41)$$

At first one might think that $\Delta\Gamma$ remains constant in time for a Hamiltonian system on account of Liouville's theorem. However, for a strongly chaotic system this notion conflicts with the finite resolution of any measurement, ultimately with the quantum uncertainty limit \hbar^N . The occupied phase space volume $\Delta\Gamma$ must, therefore, be smeared out with the finite resolution:

$$\Delta\Gamma \rightarrow \overline{\Delta\Gamma}, \quad S = \ln(\overline{\Delta\Gamma}) + \text{const.}, \quad (42)$$

a process usually referred to as *coarse-graining*. For a strongly chaotic, or mixing system the instability of trajectories leads to a growing filamentation of the phase space volume occupied by an ensemble, as illustrated in Figure 16.

Figure 16. Filamentation of the occupied phase space volume permits a chaotic system to “fill” the available phase space homogeneously without violating Liouville's theorem (from Zaslavsky⁶⁴).

A careful analysis⁶⁴ of this process shows that the coarse-grained entropy of a strongly chaotic system grows linearly with time:

$$ds/dt = \langle h \rangle_{\Gamma}, \quad (43)$$

where the right-hand side denotes the phase-space average of the sum of all positive Lyapunov exponents:

$$h = \sum_{\alpha} \lambda_{\alpha} \theta(\lambda_{\alpha}). \quad (44)$$

In this way entropy growth, and ultimately thermalization, in classical dynamical systems is intimately connected to the instability of its trajectories in phase space.

One may ask whether this has any relevance for quantum systems? Intuitively, one would suppose that it must, because highly excited states of a quantum system

* The constant is undefined in classical physics; its value is fixed when the volume $\Delta\Gamma$ is measured in units of \hbar^N , where N is the number of degrees of freedom.

usually exhibit many aspects of classical dynamics. However, the notion of a Lyapunov exponent has no immediately counterpart in quantum mechanics, because one cannot define a trajectory in phase space for quantum mechanics. Recently, however, Gun He has pointed out that there exists a closely related concept in quantum mechanics, namely the growth of local inhomogeneities in the Wigner function of an ensemble of quantum systems⁶⁵. In simple, analytically tractable examples one finds that the exponential growth of the variance of this generalized phase space distribution is governed by the same exponent as the divergence of trajectories in the classical system. This can be utilized to introduce a meaningful concept of entropy for quantum systems that differs from von Neumann's information entropy, but provides a useful description of the approach to equilibrium⁶⁵.

Now back to QCD! It has been known for a long time that non-abelian gauge theories exhibit elements of chaos in the classical limit⁶⁶. Recently, Trayanov and myself showed⁶⁷ that randomly chosen field configurations in SU(2) lattice gauge theory are characterized by a universal Lyapunov exponent, which scales with the average energy density. This analysis has been extended to SU(3) by C. Gong⁶⁸, who found the result

$$h \simeq \frac{1}{10} g^2 \langle E_p \rangle, \quad (45)$$

where $\langle E_p \rangle$ denotes the average energy per lattice plaquette. For a thermalized system the relation $\langle E_p \rangle = \frac{16}{3} T$ holds in SU(3); hence one obtains an entropy growth rate for SU(3) gauge theory of

$$dS/dt = \langle h \rangle \simeq 0.54 g^2 T. \quad (46)$$

This value coincides numerically with (twice) the thermal damping rate of long-wavelength gluons

$$\gamma_g^{(0)} = \frac{6.635}{4\pi} g^2 T \simeq 0.264 g^2 T. \quad (47)$$

The factor two between (46) and (47) may be understood by the remark that (47) gives the damping rate of the gluon *amplitude*; the decay rate of the probability is $2\gamma_g$. Although it is easy to see similarities between $\langle h \rangle$ and $2\gamma_g$, their identity has not been established, and their numerical equality may be accidental. Independent of this, however, eq. (46) provides us with a precise value of the gluon thermalization time in the high-temperature, classical limit, defined as the characteristic entropy growth time near equilibrium:

$$\tau_s = \langle h \rangle^{-1} \simeq 1.85/g^2 T. \quad (48)$$

Using the one-loop expression for the running thermal coupling constant

$$g^2(T) = \frac{16\pi^2}{11 \ln(\pi T/\Lambda)^2} \quad (49)$$

one finds thermalization times of the order of 0.4 fm/c, as shown in Figure 17. This value is comfortably short on the time-scale of relativistic heavy ion collisions, where the high-density phase is predicted to last for several fm/c.

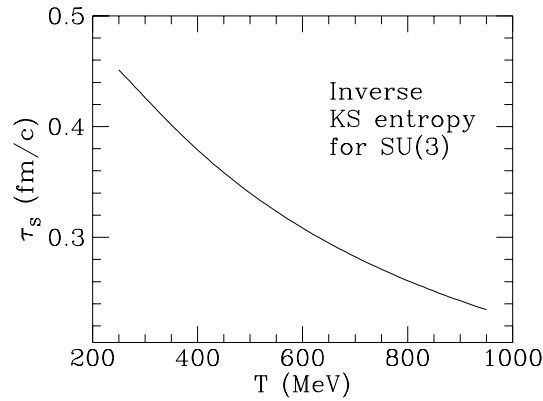


Figure 17. Thermalization time of gluonic matter close to thermal equilibrium, as obtained from the Lyapunov exponent of thermal SU(3) lattice gauge theory⁶⁸.

The advantage of the definition (48) of the thermalization is that it is also meaningful for field configurations that are far from the average thermal configuration. Numerical studies of the rate of instability of coherent field configurations in SU(2) gauge theory have yielded even higher rates of entropy growth for the same energy density⁶⁷. More general investigations of this phenomenon would be helpful.

FORMATION OF THE QUARK-GLUON PLASMA

Approaches to the Thermalization Problem

In the previous section we discussed how the quark-gluon plasma equilibrates when it is already close to thermal equilibrium. Relativistic heavy ion collisions pose a very different problem: how do the fully coherent parton wave functions of two nuclei in their ground states evolve into locally quasi-thermal distributions of partons as they are characteristic of the quark-gluon plasma state? There are mainly two approaches to this problem that have been extensively investigated: (a) QCD string breaking and (b) the partonic cascade.

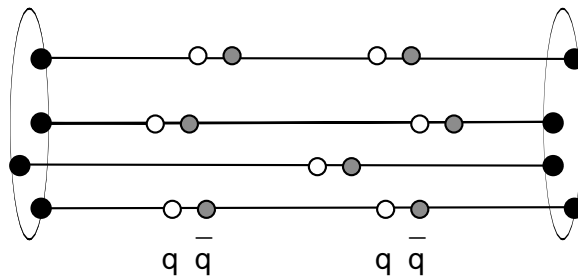


Figure 18. String-based picture of the formation of a quark-gluon plasma. Primary interactions lead to color flux tubes which break by quark pair production.

In the string picture, developed from models of soft hadron-hadron interactions, one assumes that nuclei pass through each other at collider energies with only a small

rapidity loss (on average about one unit), drawing color flux tubes, or strings, between the “wounded” nucleons. If the area density of strings is low (not much greater than 1 fm^{-2}) they are supposed to fragment independently by quark pair production on a proper time scale of order $1 \text{ fm}/c$. Most realizations of this picture are based on the Lund string model⁶⁹, e.g. Fritiof⁷⁰, Attila⁷¹, Spacer⁷², Venus⁷³, QGSM⁷⁴ and RQMD⁷⁵. When the density of strings grows further, at very high energy and for heavy nuclei, the formation of “color ropes” instead of elementary flux tubes has been postulated⁷⁶.

Alternatively, a continuum description based on the Schwinger model of (1+1)-dimensional QED with heuristic back-reaction—“chromohydrodynamics”—has been invoked to describe the formation of a locally equilibrated quark-gluon plasma^{77,78}. One general aspect of these models is that initially part of the kinetic energy of the colliding nuclei is stored in coherent glue field configurations, which subsequently decay into quark pairs. The flux tubes carry no identifiable entropy. The entropy associated with a thermal state is produced in the course of pair creation. In particular, there is no distinction between gluon and quark thermalization.

Figure 19. Schematic view of a parton cascade (from ref. 85).

The parton cascade approach, whose basic concepts were developed by Boal⁷⁹, Hwa and Kajantie⁸⁰ and Blaizot and A. Mueller⁸¹, is founded on the parton picture and renormalization-group improved perturbative QCD. Whereas the string picture runs into conceptual difficulties at very high energy, when the string density becomes large, the parton cascade becomes invalid at lower energies, where most partonic scatterings occur at energies that are too low to be described by perturbative QCD. Nevertheless, the two descriptions may well be just two different formulations of the same physical processes, since there exists a remarkable similarity between the states produced by QCD bremsstrahlung and QCD flux tubes⁸².

Let us look at the “big picture”, illustrated in Figure 20, where we distinguish three regimes in the evolution of an ultra-relativistic heavy-ion collision. Immediately after the Lorentz contracted nuclear “pancakes” have collided, scattered partons develop an incoherent identity and evolve into a quasithermal phase space distribution by free streaming separation of the longitudinal spectrum (a). Rescattering of these partons finally leads to the thermalization after a time of the order of $1 \text{ fm}/c$. The thermalized quark-gluon plasma then evolves according to the laws of relativistic hydrodynamics (b), until it has cooled to the critical temperature $T_c \simeq 150\text{-}200 \text{ MeV}$, where it begins to hadronize (c). The physics governing the evolution during the three stages is very different. In this section we will concentrate mainly on the first, i.e. the preequilibrium state, because it is here where much recent progress has been made in our understanding.

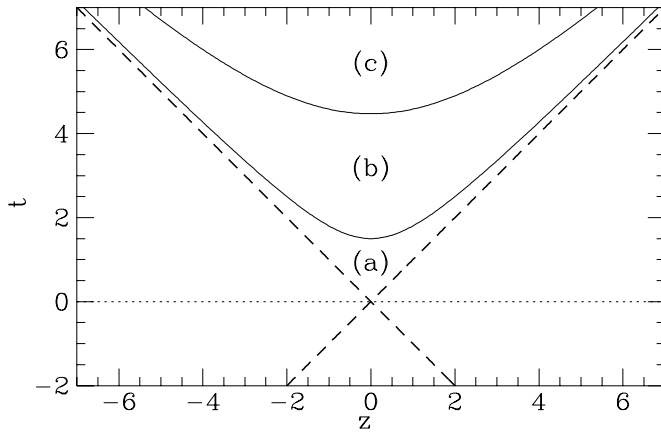


Figure 20. One-dimensional space-time picture of the evolution of an ultrarelativistic nuclear collision, distinguishing three regimes: (a) Pre-equilibrium state, (b) thermalized quark-gluon plasma, (c) hadronization phase. z denotes the beam axis. The dashed lines indicate the colliding nuclei.

Parton Cascades

As mentioned above, a fast parton of energy E_p penetrating a quark-gluon plasma loses about 1 GeV of energy in every 1 fm traversed. Its thermalization is therefore of the order

$$\tau_{\text{th}} = \left(\frac{E_p}{\text{GeV}} \right) \text{ fm}/c, \quad (50)$$

which can be many tens or hundreds of fm/c for a fast parton. How, then, is it possible that two nuclei colliding at 100 GeV/u (RHIC) or 3000 GeV/u (LHC) can deposit enough energy while penetrating each other to thermalize within 1 fm/c proper time? The resolution of this almost paradoxical situation has two aspects:

- (a) The emphasis is on *proper time* τ . $\tau = 1$ fm/c corresponds to a very long time in the laboratory frame for matter produced at high rapidity. To wit, thermalization measured in the rest frame of the fast parton takes only

$$\tau_{\text{th}} = \int \frac{dt}{\gamma_p} = \int \frac{m_p^*}{E_p} \frac{dE_p}{|dE/dx|} = \frac{m_p^*}{|dE/dx|} \ln(E_p/3T) \quad (51)$$

where m_p^* is the effective parton mass, and $3T$ is the average thermal energy of a parton.

- (b) Nucleons contain partons of all possible energies. Soft partons, i.e. partons with $x \ll 1$ mainly contribute to matter formed at central rapidity in the c.m. frame, while hard partons, i.e. those with $x \simeq 0.3 - 1$, are the source of matter at large rapidity in the c.m. frame. It is quite illuminating to consider what would happen, if it were possible to instantaneously “shatter” the complete parton wave function of a fast nucleon. Indeed, one may ideally think of the collision of two nuclei at ultrarelativistic energies as an event during which only the phase coherence of the initial parton distributions is almost totally destroyed, but their longitudinal momentum distribution remains rather unchanged. Let us see, therefore, what would happen if the nuclear collision acts as such a “phase filter.”⁸³

Intermezzo: Nuclear Collisions as “Phase Filter”

We calculate the rapidity distributions of those quantities of the parton distribution which are relevant to experimental data regarding the final state. One candidate is the entropy distribution, dS/dy , the other is the rapidity distribution of transverse energy, dE_T/dy . For the calculation of dS/dy and dE_T/dy let us consider the phase space density of partons of flavor i with degeneracy d_i :

$$f_{i,A}(\vec{P}, \vec{r}) = \frac{(2\pi)^3}{d_i} \frac{dN_A}{d^3p d^3r} = \frac{(2\pi)^3}{d_i} \frac{1}{V_A^*} \frac{dN_A}{d^3p}. \quad (52)$$

Here A denotes the mass number of the colliding nuclei and V_A^* is the effective nuclear volume to be specified below. The momentum dependence of phase-space density can be derived from the measured parton structure functions:

$$\frac{dN_a}{d^3p} = \frac{1}{P} \tilde{F}_{i,A}(x, p_T^2) \approx \frac{1}{P} A F_i(x) \frac{1}{2\pi p_0^2} \exp(-p_T^2/2p_0^2) \quad (53)$$

where we assumed the factorization of the longitudinal and transverse momenta: x is the Bjorken variable, the fraction of the nucleon’s longitudinal momentum P carried by a parton. $F_i(x)$ is the measured parton distribution in the nucleon, where shadowing effects are neglected here. One normally assumes a Gaussian distribution of width $p_0 \simeq 0.3$ GeV/c for the transverse parton momenta.

To determine the spatial dependence of the phase space density, we use the concept of *distributed contraction* of partons⁸⁰. Let us call Y the beam rapidity and y the parton rapidity in the c.m. system. Then only those partons occupy the Lorentz contracted region of fast moving nucleons with radius R_N which satisfy the uncertainty relation

$$p_L \cdot \frac{2R_N}{\cosh Y} \geq \frac{1}{2}. \quad (54)$$

Here p_L is the longitudinal momentum of the parton and $R_N/\cosh Y = R_N/\gamma$ is the longitudinal size of the contracted nucleons. Partons with smaller longitudinal momenta than (54) are more spread out in the longitudinal direction to satisfy the Heisenberg uncertainty relation, they form a cloud, containing mostly gluons and sea-quarks, surrounding the contracted nucleons (see Figure 21).

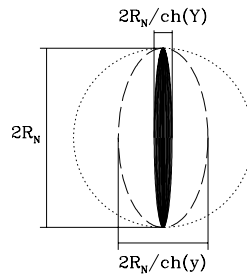


Figure 21. The longitudinal spread of the distributions of partons with rapidity y around a Lorentz contracted proton moving with rapidity Y . The spread is determined by the uncertainty relation.

The effective spatial volume is then:

$$V_A^*(y) = \frac{4\pi R_A^2}{3} \frac{R_N}{\cosh \tilde{y}}, \quad (55)$$

where $\tilde{y} = \min(y, Y)$. One obtains a critical value $x_c = \cosh Y / (4R_N P) \approx 0.1$. For $x \leq x_c$ distributed contraction sets in. Considering the phase-space element

$$\frac{d^3 p d^3 r}{(2\pi)^3} = \frac{V_A^*(y)}{(2\pi)^2} p_T^2 dp_T \cosh y, \quad (56)$$

we can now calculate the rapidity distributions:

$$\frac{dS}{dy} = \int_0^\infty \frac{dp_T}{(2\pi)^2} V_A^* p_T^2 \cosh y \sum_i d_i [f_i \ln f_i - (1 \pm f_i) \ln(1 \pm f_i)], \quad (57)$$

$$\frac{dE_T}{dy} = \int_0^\infty \frac{dp_T}{(2\pi)^2} V_A^* p_T^3 \cosh y \sum_i d_i f_i, \quad (58)$$

where

$$f_i = \frac{1}{d_i} \frac{(2\pi)^3}{V_A^* P} A F_i(x) \frac{1}{2\pi p_0^2} \exp(-p_T^2 / 2p_0^2). \quad (59)$$

Using the approximation, $\sum_i F_i(x) \approx D/x$ for sea partons, one obtains the following expression for the integral (58):

$$\frac{dE_T}{dy} = \frac{ADp_0 \sqrt{\pi/2}}{\tanh y}. \quad (60)$$

The evaluation of dS/dy is more complicated and it is not expected to be linear in A , but it only depends on $\tanh y$, as well. These results mean that the concept of “*phase filtering*” leads to the prediction of a boost invariant phase-space distribution of partons in the rapidity region $1 < y < Y$, where $\tanh y \simeq 1$, as it was postulated by Bjorken⁸⁴. In the region $0 < y < 1$ we have a strong rapidity dependence in expressions (57,58), because the function $(\tanh y)^{-1}$ diverges in the limit $y \rightarrow 0$. However, a detailed analysis⁸³ shows that this is balanced by the need to introduce a lower cut-off in the p_T integrations, allowing for the continuation of the constant rapidity distributions down to $y = 0$.

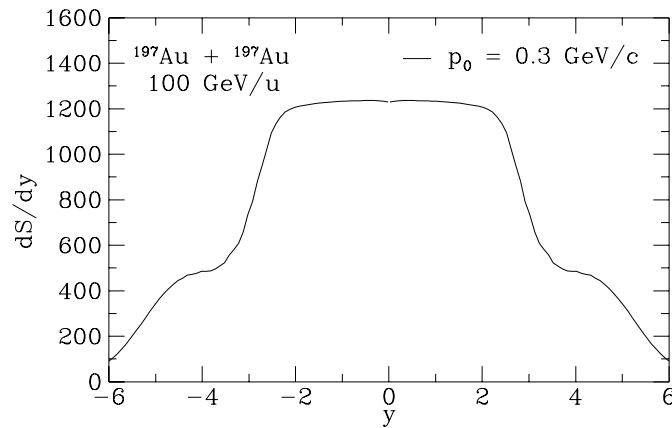


Figure 22. Rapidity distributions of partons in collisions at RHIC (Au+Au at E_{cm} ($A=100$ GeV), assuming complete “*phase filtering*” of the initial distributions. p_0 parametrizes the initial transverse momentum distribution of partons in the nucleon.

Let us consider a Au+Au collision at the characteristic energy of the Brookhaven RHIC machine (100 GeV/u), for which our considerations are likely to be applicable.

As seen in Figure 22 an extended central plateau develops, where we predict a hadron multiplicity $dN/dy > C^{-1}(dS/dy) = 400$, with $C \simeq 3.6$ for a thermal ultra-relativistic Bose gas. This multiplicity may rise further due to rescattering and fragmentation. These effects can be studied systematically in a complete parton cascade model⁸⁵, as we will discuss further below.

Parton Cascades (continued)

Having discussed the initial parton structure of the colliding nuclei, let us examine the scattering event more closely. When the two Lorentz-contracted nuclei collide, some of the partons will scatter and then continue to evolve incoherently from the remaining partons. Three aspects of these individual parton scatterings are worth discussing:

- (a) A parton-parton scattering can be described by perturbative QCD, if the momentum transfer involved is sufficiently large. Nobody knows for sure where perturbative QCD becomes invalid, but typical choices^{85–87} for the momentum cut-off are $p_T^{\text{min}} \simeq 1.7\text{-}2$ GeV/c.
- (b) The elementary scattering has a finite space-time duration, which is given by the amount of off-shell propagation of exchanged virtual gluons or quarks. For the typical momentum transfer $p_T = p_T^{\text{min}}$ this range is

$$\Delta t, \Delta x \simeq 1/p_T^{\text{min}} \simeq 0.1 \text{ fm}/c. \quad (61)$$

More precisely, this estimate applies to the QCD diagrams involving t -channel exchange, which dominate the total parton cross-section. For s -channel diagrams, e.g. $\bar{q}q$ annihilation into a lepton pair, the elementary time scale is of order $\hat{s}^{-1/2}$, the inverse scattering energy in the parton c.m. frame.

- (c) The time it takes for the scattered parton wave functions to decohere from the initial parton cloud depends on the transverse momenta of the scattered partons. Usually, one argues that the partons must have evolved at least one-half transverse wavelength $\lambda_T = \pi/p_T$ away from their original position before they can be considered as independent quanta. The considerations underlying this argument are similar to those for the Landau-Pomeranchuk effect^{60,61}. The critical issue here is that parton-parton cross sections are defined as squares of S-matrix elements which involve integration over all space and time from the infinite past to the infinite future. In the course of the nuclear interaction, however, that integration cannot be extended beyond their previous interaction point or their point of “formation”. If the plane wave factors representing the partons have not performed at least one-half complete oscillation the limited integral is not reasonably well represented by an S-matrix element. This is probably the weakest point in the line of arguments for a parton cascade and clearly would warrant more careful study.

In any event, one concludes that a minimal time of the order of 0.1-0.3 fm/c must pass before scattered partons can be considered as incoherent field quanta, which fully contribute to the entropy and can rescatter as independent particles.

What happens after the initial scattering? The longitudinal parton momentum is little changed on average, i.e. $p'_z \simeq p_z = xP$, hence the scattered parton appears at rapidity

$$y \simeq \ln(2p_z/p'_T), \quad (62)$$

where p'_T is its final transverse momentum. Let us recall that the partons with momentum p_z were originally localized in a longitudinal interval (see Figure 20):

$$\Delta z \simeq \frac{1}{2p_z} \simeq \frac{1}{p'_T e^y}. \quad (63)$$

Hence, immediately after the nuclei have collided, the fast partons are highly localized, whereas the distribution of soft partons is more fuzzy. Now let us make the outrageous assumption that the cloud of once scattered partons expands without any further interaction! Obviously, this implies the gradual separation of partons according to their velocity, because fast partons will leave the original interaction site quickly, while slower partons stay behind. Because of the approximate boost invariance already present in the initial state, we restrict the following discussion to the central rapidity interval, say, $-1 < y < 1$. In particular all partons with momenta greater than $|p_z|$ will have moved away from the central plane $z = 0$ after a time

$$\tau(p_z) = \frac{\Delta z}{v_z} \simeq \frac{1/2 p_z}{p_z/E} = \frac{\sqrt{p_z^2 + p_T'^2}}{2p_z^2}. \quad (64)$$

Hence the longitudinal momentum spread of partons remaining at $z = 0$ drops rapidly. It becomes equal to the average transverse momentum after:

$$\tau(p_z \simeq \langle p_T' \rangle) = \frac{1}{\sqrt{2} \langle p_T' \rangle} \simeq \frac{1}{1.4 \text{ GeV}/c} = 0.15 \text{ fm}/c, \quad (65)$$

where we have assumed an average transverse momentum of 1 GeV/c, in line with results of numerical simulations^{85,86}.

At that moment the distribution of scattered partons in the most central slab ($z \simeq 0$) is approximately isotropic. It is also approximately *thermal*? That depends on the actual *phase space density* of partons in the vicinity of $z = 0$. Only if every phase space cell up to $|\vec{p}| \simeq \langle p_T' \rangle$ is occupied with probability close to one, can we speak of a quasi-thermal distribution. So let us estimate the phase space density. According to eq. (62), counting only the gluon distribution $G(x)$, the number of partons in the original nuclear distributions, per unit of rapidity, is:

$$\frac{dN}{dy} \simeq \frac{dN}{d(\ln x)} \simeq 2AxG(x) \xrightarrow{x \rightarrow 0} = 6A. \quad (66)$$

Here we have neglected nuclear shadowing, since we are aiming at a crude estimate. Let us further assume that the nuclei are sufficiently “thick” and the collision energy is high enough that most available partons actually are scattered. The gluon phase space volume to be occupied is:

$$\frac{dV_p}{dy} = 16\pi R_A^2 \Delta z \frac{\Delta p_z}{dy} \frac{\pi \langle p_T'^2 \rangle}{(2\pi)^3}, \quad (67)$$

where the factor 16 counts the color-spin degeneracy and $R_A = r_0 A^{1/3}$ stands for the nuclear radius. From the uncertainty relation (63) we have $\Delta z \cdot \Delta p_z \simeq 1$; and since we have waited until Δp_z has become equal to $\langle p_T' \rangle$, the rapidity spread of partons is $\Delta y \simeq 1$. Combining everything, we find

$$dV_p/dy \simeq \frac{2}{\pi} R_A^2 \langle p_T'^2 \rangle. \quad (68)$$

Asking for full phase space occupation means requiring $dV_p/dy \leq dN/dy$, or

$$A^{1/6} \geq \frac{r_0 \langle p_T' \rangle}{\pi} \simeq 2, \quad (69)$$

i.e. $A \geq 50$, if we use $\langle p'_T \rangle \simeq 1$ GeV/c. Of course, not every available gluon from the initial structure functions will scatter when the nuclei collide. On the other hand, the fragmentation of scattered partons due to gluon bremsstrahlung effectively increases the number of scattered partons. Quantitative predictions can be made using a complete simulation of perturbative parton interactions, such as the parton cascade⁸⁵ or HIJING⁸⁷. A calculation with HIJING for the system Au + Au at LHC energy was reported in ref. 88. The result was $dN/dy \simeq 800$, $\langle p'_T \rangle \simeq 1.75$ GeV/c. The available phase space, according to eq. (68) is:

$$\frac{dV_p}{dy} = \frac{2}{\pi} \left(\frac{6\text{fm} \cdot 1.75\text{GeV}}{0.2\text{GeV fm}} \right)^2 \simeq 1500, \quad (70)$$

i.e. phase space is about half occupied on average. The situation is less favorable with smaller nuclei or at lower energies. Figure 23 shows the number of primary parton-parton collisions for nucleon-nucleon collisions as well as for collisions of medium-sized

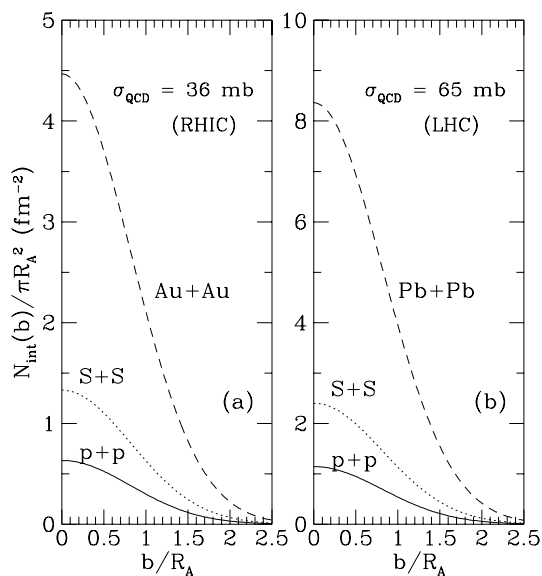


Figure 23. Area density of primary parton scatterings for various projectiles at RHIC and LHC energies, as a function of the reduced impact parameter b . R_A denotes the projectile radius.

and heavy nuclei, respectively, in the RHIC and LHC energy ranges⁸⁶. The advantage of heavy nuclei, such as Au or Pb, for achieving a high density of scattered partons is obvious. Sulfur nuclei do not bring a great improvement over central nucleon-nucleon interactions. The increase in c.m. energy between RHIC and LHC by a factor 30 brings about a considerable increase in the parton density, as shown in Figure 24. The rise is not only due to the increased number of primary scatterings, but also partially caused by the growing amount of initial- and final-state gluon radiation. The calculations also show that only a small fraction of scattered partons are quarks. The assumption of fully thermalized quark distributions at very early times, $\tau \ll 1$ fm/c, is therefore most likely unwarranted⁸⁹.

Complete calculations following the evolution of the parton distributions microscopically until the attainment of thermal equilibrium have been carried out recently by K. Geiger^{85,91}. A detailed account of these is given in Geiger's lecture at this School. Suffice it to mention here that he finds almost fully thermalized phase space

distributions of gluons in Au + Au collisions at RHIC energy ($E_{cm} = 100$ GeV/u) with $T \simeq 325$ MeV after proper time $\tau \simeq 1.8$ fm/c (see Figure 25). If this captures the truth, there can be no doubt that a quark-gluon plasma will be observed in experiments at RHIC.

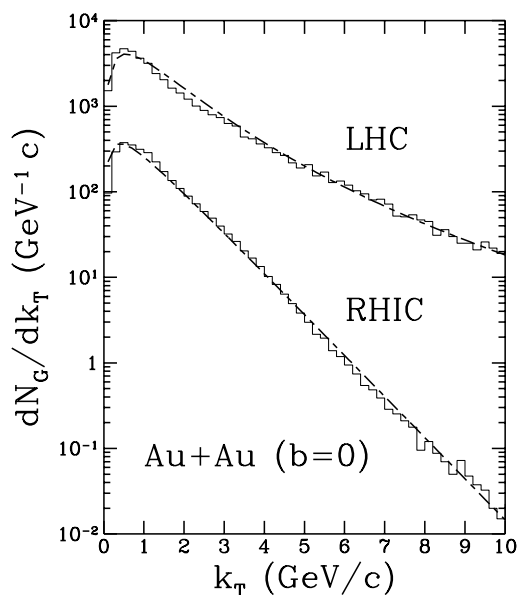


Figure 24. Distributions of scattered gluons predicted by HIJING for Au+Au collisions at RHIC and LHC. The predictions contains elementary QCD scattering cross sections and the radiative cascades of final state partons in the leading logarithmic approximation⁸⁶.

Figure 25. Rapidity and transverse momentum distribution of final-state partons as predicted by the parton cascade⁹¹. The values of T are obtained by a fit of the analytical isotropic fireball formula to the numerical results.

Pre-Equilibrium Parton Physics

The complete spectrum of phenomena occurring during the approach toward local thermal equilibrium still awaits exploration. Here I will discuss just two aspects: color screening⁸⁸ and charm production⁹², because they are dominated by the

evolution of the gluon distribution, which is better understood at this moment. The experimentally very interesting contribution to lepton-pair production, which has also been studied⁹³, is more sensitive to the quark distribution.

*Color screening*⁸⁸: The screening length λ_0 of longitudinal color fields is important, because it defines the range over which coherent color-electric fields can extend. If it is larger than the characteristic confinement radius $\Lambda^{-1} \simeq 1$ fm, long-range color-electric fields arrange themselves as flux tubes. In the one-loop approximation, λ_D is determined by the momentum distribution $f(\mathbf{k})$ of gluons according to:

$$\lambda_D^{-2} = -\frac{3\alpha_s}{\pi^2} \lim_{|\mathbf{q}| \rightarrow 0} \int d^3k \frac{|\mathbf{k}|}{\mathbf{q} \cdot \mathbf{k}} \mathbf{q} \cdot \nabla_{\mathbf{k}} f(\mathbf{k}). \quad (71)$$

A simple result can be obtained when the gluon distribution is exponential in k_T and flat in rapidity y :

$$\lambda_D^{-2} \simeq \frac{3\pi\alpha_s}{R_A^2 \tau \langle k_T \rangle} \frac{dN}{dy}, \quad (72)$$

where dN/dy is the rapidity density of gluons. At the earliest time $t_i \simeq \langle k_T \rangle^{-1}$, when the scattered gluons become incoherent, the calculations of ref. 88 based on the HIJING code predict

$$\begin{aligned} \lambda_D &\simeq 0.4 \text{ fm} && \text{(RHIC),} \\ \lambda_D &\approx 0.15 \text{ fm} && \text{(LHC).} \end{aligned} \quad (73)$$

We conclude that the color screening length at LHC energies will be so short, even after the first sequence of parton interactions, that coherent flux tubes cannot develop. The Lund model with its formation of independent strings that break up by creation of quark pairs is simply not applicable under these conditions. At RHIC, on the other hand, the screening length appears to be marginally favoring a parton cascade description, but models with partially fusing flux tubes (“color ropes”) may also be able to describe certain aspects of the pre-equilibrium phase of the nuclear collision.

*Charm production*⁹²: Charmed quark pairs are predominantly produced in collisions between two gluons. Since the charm production threshold is rather high, about 3 GeV, the rate of production in a thermalized quark-gluon plasma with temperature $T \simeq 300$ MeV is negligible. Conventional wisdom until recently was, therefore, that most charmed quarks are produced in primary parton interactions⁹⁴. In view of the high density of scattered partons with transverse momenta well above 1 GeV at collider energies, one may suspect that there is a sizable contribution to charm production from secondary parton collisions. This is borne out by a calculation of secondary charm production based on the initial scattered gluon distribution predicted by HIJING⁹². The additional charmed quarks populate predominantly the central rapidity plateau, where initial charm production is reduced by gluon shadowing effects (see Figure 26). At LHC energies the total yield of secondary charmed quarks may be twice as large as that of primary charmed quarks.

The amount of secondary charm production is sensitive to the thermalization time of the parton distribution. It depends on the ratio $\langle \sigma_c \rangle / \langle \sigma_{\text{tot}} \rangle$, where $\langle \sigma_{\text{tot}} \rangle$ is the average total parton-parton cross section that governs thermalization, while $\langle \sigma_c \rangle$ denotes the averaged cross section for charm production. $\langle \sigma_{\text{tot}} \rangle^{-1}$ is proportional to the thermalization time τ_{th} . A measurement of the total yield of charmed particles (mostly D-mesons) in the central rapidity region would, therefore, provide valuable information on the time-scale of thermalization⁹².

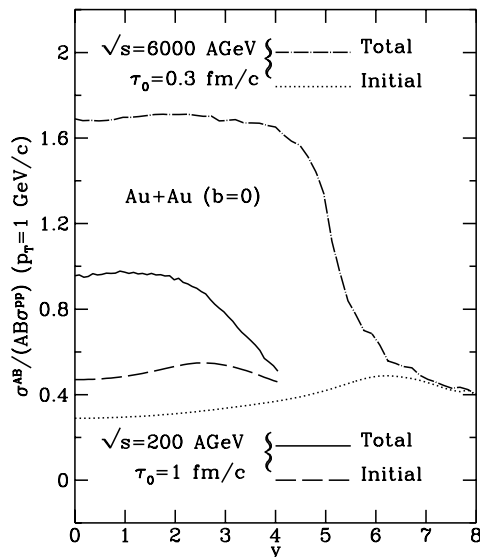


Figure 26. Rapidity distributions of charmed quarks produced in secondary gluon interactions, in comparison to the primary parton model predictions. The calculations are based on Duke-Owens structure functions with nuclear gluon shadowing.

Plasma Evolution and Hadronization

Once the quark-gluon plasma has reached local thermal equilibrium, its further evolution can be described without reference to the parton reactions at the microscopic level. This concept was first quantitatively developed by Bjorken⁸⁴. The hydrodynamic equations for an ultrarelativistic plasma with $P = \frac{1}{3}\varepsilon$ admit a boost-invariant solution describing a longitudinally expanding fireball with constant rapidity density. When transverse expansion effects are taken into account, longitudinal boost invariance is partially destroyed, but the overall picture remains intact. This scenario has been thoroughly studied by a large number of theorists. Because the results are accessible in several fine reviews⁹⁵, I will refrain from discussing it here in detail.

An important aspect of the late evolution of the quark-gluon plasma is its hadronization. Mostly it is assumed that the plasma expands and cools until it reaches the critical temperature $T_c \simeq 200\text{MeV}$ and then converts into a hadronic gas while maintaining thermal and chemical equilibrium. More detailed descriptions of the dynamics of hadronization have been developed in connection with the problem of strangeness production, which is reviewed in the next chapter.

A totally different approach, explored only very recently, consists in following the partonic reactions at a microscopic level, until the parton density has become sufficiently low to permit the formation of individual hadrons⁹¹. A great deal is known about the mechanism of final state hadron production in e^+e^- and NN-scattering but, unfortunately, we do not know whether this knowledge applies to the hadronization of a quark-gluon plasma in bulk. Therefore, the treatment of hadron formation at the end of a partonic cascade is fraught with a great deal of uncertainty.

At present, it is hard to judge the merits of either approach on a theoretical basis. Their validity and usefulness simply depends on whether the microscopic processes during hadronization proceed approximately at thermodynamical equilibrium or not. The lesson from nuclear collision processes at much lower energies (below 1

GeV/u) has been that both scenarios are possible: neutron evaporation from highly excited nuclear fragments is well described by thermodynamics, but nuclear multi-fragmentation, where Coulomb forces play a dominant role, requires a more detailed theoretical treatment.

QUARK-GLUON PLASMA SIGNATURES

All theory of the quark-gluon plasma would be largely academic if there were no reliable signatures to observe its formation and to study its properties experimentally. It is impossible to present a complete review of quark-gluon plasms signatures here. I will, therefore, only try to capture the essential ideas and the current status of the theoretical studies on the most promising quark-gluon plasma signals. Anyone interested in more details is referred to the review of Kajantie and McLerran⁹⁶ and to the proceedings of the Strasbourg workshop⁹⁷.

In order to shed some light on the connections between the many proposed quark-gluon plasma signatures I will group them in five categories, according to the physical properties of superdense hadronic matter to which they are sensitive. These are:

1. thermodynamic variables measuring the equation of state;
2. probes for chiral symmetry restoration;
3. probes of the color response function;
4. probes of the electromagnetic response function;
5. “exotic” signatures of the quark-gluon plasma.

Thermodynamic Variables

The basic idea behind this class of signatures is to measure the equation of state of superdense hadronic matter, i.e. the dependence of energy density ϵ , pressure P , and entropy density s on temperature T and baryochemical potential μ_B . Here one wants to search for a rapid rise in the effective number of degrees of freedom, as expressed by the ratios ϵ/T^4 or s/T^3 , over a small temperature region. These quantities would exhibit a discontinuity, if there were a first-order phase transition, and if we were dealing with systems of infinite extent. More realistically, we can expect a steep, step-like rise. According to recent lattice simulations this rise should occur over a temperature range of less than 10 MeV.

Of course, one requires measurable observables that are related to the variables T , s , or ϵ . It is customary to identify those with the average transverse momentum $\langle p_T \rangle$, and with the rapidity distribution of hadron multiplicity dN/dy , or transverse energy dE_T/dy , respectively⁹⁸. One can then, in principle, invert the $\epsilon - T$ diagram and plot $\langle p_T \rangle$ as function of dN/dy or dE_T/dy . If there occurs a rapid change in the effective number of degrees of freedom, one expects an S-shaped curve, as shown in Figure 27, whose essential characteristic feature is the saturation of $\langle p_T \rangle$ during the persistence of a mixed phase, later giving way to a second rise when the structural change from color-singlet to colored constituents has been completed. Detailed numerical studies in the context of the hydrodynamical model have shown that this characteristic feature is rather weak in realistic models, unless rehadronization occurs like an explosive process⁹⁹.

In order to trace this curve in nuclear collisions one probably has to vary the beam energy in rather small steps. This has not been done, so far, but it will be possible at RHIC. In nucleon-antinucleon collisions, however, one may make use of the existence of large fluctuations in the total multiplicity even from central $N - N$ collisions. Using this tool, the E-735 collaboration at Fermilab¹⁰⁰ found a continued

rise of $\langle p_T \rangle$ for antiprotons and hyperons with multiplicity, reaching 1 GeV/c for the most violent events ($dN/dy > 20$). When these data are analyzed in terms of a simple model, where one assumes that all hadrons are emitted from a longitudinally and transversely expanding fireball¹⁰¹, one finds that the surface velocity at high dN/dy must take on quite large values for the hadrons, reaching up to $v/c = 0.8$. Studying the hydrodynamical evolution that might lead to this final state, it is hard to believe that such a “flow” pattern can be produced at the level of hadrons, because the drag exerted by the dominant pions on the nucleons is far too weak to accelerate these to such speed.

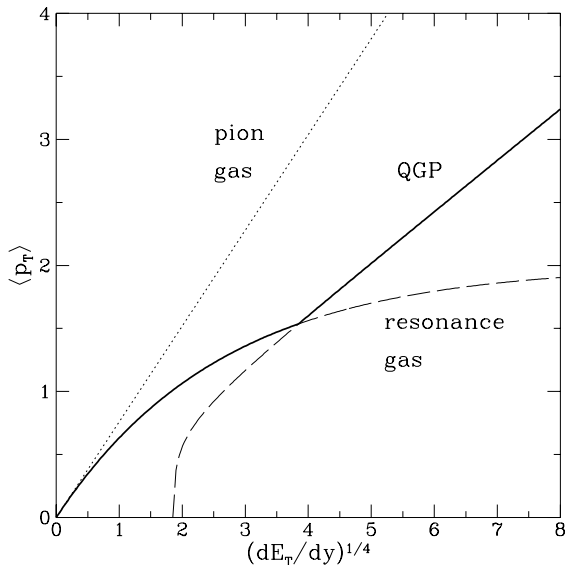


Figure 27. Average transverse momentum of emitted hadrons as function of transverse energy dE_T/dy , representing the maximal energy density reached in a collision. The different curves correspond to: (a) pion gas, (b) Hagedorn resonance gas, (c) quark-gluon plasma.

The question then is: What produces the apparent transverse flow? Clearly, it must be established at the quark-parton level. It could be a consequence of expansion of a quark-gluon plasma or mixed phase. This could be tested by inspection of the full p_T spectra at high multiplicity¹⁰². Alternatively, the transverse “flow” might be generated by the superposition of several extended minijets, as argued by Gyulassy and Wang¹⁰³. It is not entirely clear that the two pictures are substantially different. Minijets might be the microscopic mechanism by which the transverse expansion of a quark-gluon plasma is produced.

Models of the space-time dynamics of nuclear collisions need independent confirmation, especially concerning the correctness of their geometrical assumptions. Such a check is provided by identical particle interferometry, e.g. of $\pi\pi$, KK , or NN correlations¹⁰⁴, which yield information on the reaction geometry. By studying the two-particle correlation function in different directions of phase space, it is possible to obtain measurements of the transverse and longitudinal size, of the lifetime, and of flow patterns of the hadronic fireball at the moment where it breaks up into separate hadrons. The transverse sizes found in heavy ion collisions¹⁰⁵, as well as in $N - \bar{N}$ collisions at high multiplicity¹⁰⁰ are larger than the radius of the incident particle, clearly exposing the fact that produced hadrons rescatter before they are finally emitted. If interferometric size determinations would be possible on an event-by-event basis when

Pb or Au beams become available, the correlation of global parameters like $\langle p_T \rangle$ and dN/dy with the fireball geometry could be performed for each individual collision event. This will allow for much more precise study of the thermodynamic properties of superdense hadronic matter and may prove to be a sharp tool in the experimental search for a phase transition.

Chiral Symmetry Restoration

The two most often proposed signatures for a (partial) restoration of chiral symmetry in dense hadronic matter are enhancements in strangeness and antibaryon production. The basic argument in both cases is the reduction in the threshold for production of strange hadrons (from about 700 MeV to 300 MeV) and baryon-antibaryon pairs (from about 2 GeV to almost zero). As Rafelski pointed out over a decade ago, the optimal signal is obtained by considering strange antibaryons, which combine both signatures¹⁰⁶. The enhanced strange quark production in a chirally restored, deconfined quark-gluon plasma¹⁰⁷ leads to chemical equilibrium abundances for all strange hadrons, which would be difficult to understand on the basis of hadronic reactions alone¹⁰⁸.

It has also been pointed out that strange particles, and especially antibaryons, would be produced more abundantly, if their masses would be modified even in the hadronic phase due to medium effects¹⁰⁹. As discussed in an earlier section, the mass of K-mesons can be substantially lowered at finite baryon number density and the effective mass of antibaryons might be substantially reduced.

An enhancement of strange particle production in nuclear collisions has been observed by many experiments¹¹⁰. However, we have also learned that such an enhancement alone does not make a reliable signature for the quark-gluon plasma. Strange particles, especially K and Λ can be copiously produced in hadronic reactions before the nuclear fireball reaches equilibrium. This mechanism seems to work very efficiently at AGS—as well as SPS—energies^{111,112}. The cascade leading to enhanced K and Λ production has been studied in detail in the framework of the RQMD model, where it was found that most of the enhancement comes from πN reactions initiated by the pions produced in first NN collisions, which have a strong nonthermal spectrum¹¹¹.

Maybe the most spectacular data in this respect are those obtained by the WA85 collaboration¹¹³ at CERN, who find the following abundance ratios at mid-rapidity and for momenta $4p_T > 1$ GeV/c:

$$\begin{aligned} \bar{\Lambda}/\Lambda &= 0.13 \pm 0.03, & \bar{\Xi}/\Xi &= 0.39 \pm 0.07; \\ \Xi/\bar{\Lambda} &= 0.6 \pm 0.2, & \Xi/\Lambda &= 0.2 \pm 0.04. \end{aligned}$$

It is difficult to understand why the production of the doubly strange $\bar{\Xi}$ should be particularly enhanced in a hadronic scenario, because the medium effects are expected to act mainly on the light quark content of baryons. Lattice calculations and sum rule estimates indicate that the light $q\bar{q}$ condensate is more rapidly depleted than the $s\bar{s}$ condensate in the medium. Rafelski¹¹⁴ has argued that the observed ratios correspond to those found in a quark-gluon plasma that is about half equilibrated in its strangeness content. More recently, Rafelski and Tounsi¹¹⁵ have argued that strange baryon ratios seen by WA85 and other CERN heavy ion experiments can be consistently explained *either* by a quark-gluon plasma or hadronic gas with the parameters $T = 220$ MeV and $\mu_B = 340$ MeV. Davidson et al.¹¹⁶ have also pointed out that the ratios found by WA85 are close to those of a hadronic gas with effective volume

correction in complete chemical equilibrium. However, even if this is so, the fundamental question raised by the data is: how chemical equilibrium be attained during the short life of a hadronic fireball in any other way than through an intermediate quark-gluon plasma phase?

Recently, attempts have been made to explain the enhanced $\bar{\Lambda}$ production seen by NA35 at midrapidity in terms of new mechanisms in the framework of collision models based on the string picture. Aichelin and Werner¹¹⁷ invoke the formation of “double strings” connected to the same leading quark to enhance the production of baryons containing strange quarks in the VENUS code. H. Sorge et al¹¹⁸ introduced a mechanism for string fusion into “color ropes”⁷⁶, which break faster and more often produce strange quarks and diquarks, into the RQMD model. This leads not only to strongly enhanced $\bar{\Lambda}$ production but also to a significant increase in the prediction for the number of produced antiprotons. Unfortunately no data on \bar{p} production at the CERN-SPS are presently available to test this prediction.

Strangeness enhancement has also been seen in the ϕ -meson channel by the NA38 experiment¹¹⁹. Koch and Heinz¹²⁰ have argued that this effect can be understood as addition ϕ -production due to rescattering of secondaries, in combination with the small absorption cross section of the ϕ -meson. The required density of scatterers agrees well with that invoked for explanation of the observed J/ψ -suppression (see below).

Color Response Function

The basic aim in the detection of a color deconfinement phase transition is to measure changes in the color response function

$$\Pi_{\mu\nu}^{ab}(q^2) = \int d^4x d^4y e^{iq(x-y)} \langle j_\mu^a(x) j_\nu^b(y) \rangle. \quad (74)$$

Although this correlator is not gauge invariant (except in the limit $q \rightarrow 0$), its structure can be probed in two ways (see Figure 28):

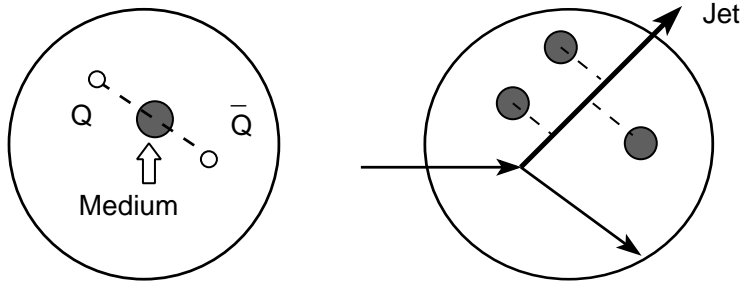


Figure 28. Medium corrections to (a) the heavy quark-antiquark potential and (b) the energy loss of a penetrating parton (QCD jet) are sensitive to the color structure of dense hadronic matter.

1. The screening length $\lambda_D \delta^{ab} = \Pi_{00}^{ab}(0)^{-1/2}$ leads to dissociation of bound states of a heavy quark pair, such as $(c\bar{c})$.
2. The energy loss dE/dx of a quark jet in a dense medium is sensitive to an average of $\Pi_{\nu\mu}^{ab}(q^2)$ over a wide range of q .

Let me begin with the energy loss of a fast quark in the quark-gluon plasma, which was first studied by Bjorken¹²¹ in perturbative QCD. The connection between

energy loss of a quark and the color-dielectric polarizability of the medium was recently investigated by several authors^{62,63} in analogy to the theory of electromagnetic energy loss. The basic formula is:

$$\frac{dE}{dx} = -\frac{C\alpha_s}{2\pi^2v} \int d^3k \omega d\omega \left[\frac{1}{k^2} \text{Im} \frac{1}{\epsilon_L} + \left(v^2 - \frac{\omega^2}{k^2} \right) \text{Im} \frac{1}{\omega^2 \epsilon_T - k^2} \right] \delta(\omega - \mathbf{v} \cdot \mathbf{k}), \quad (75)$$

where $\epsilon_{L/T}$ denote the longitudinal and transverse components of the color-dielectric given explicitly in eqs. (30). C is the Casimir operator for the color representation of the penetrating particle ($C = \frac{4}{3}$ for quarks, $C=3$ for gluons). Using eqs. (30) the expression can be evaluated analytically, yielding the energy loss of a fast quark:

$$\frac{dE}{dx} = -\frac{8\pi}{3} \alpha_s^2 T^2 (1 + N_f/6) \left[\frac{1}{v} - \frac{1-v^2}{2v^2} \ln \frac{1+v}{1-v} \right] \ln(q_+/q_-). \quad (76)$$

This result includes both single-particle collisional energy loss and energy loss through excitation of plasmons. All the medium dependence resides in the cut-off momenta q_{\pm} in the logarithm: $q_+ \approx 2\sqrt{TE}$, while q_- is a function of the Debye screening mass $m_D = \lambda_D^{-1}$ in the quark-gluon plasma phase. The magnitude of the energy loss is critically influenced by the strong coupling constant α_s , whose value unfortunately is not well known. The choices 0.2 and 0.3 preferred by various authors^{61,62} leads to a stopping power between 0.4 and 1 GeV/fm for a fast quark. This may be a little smaller than the energy loss of a fast quark in nuclear matter.

In addition, a fast quark loses energy by radiating gluons. Although this mechanism is strongly suppressed a high energy by the Landau-Pomeranchuk effect, it still contributes of the order of 1 GeV/fm to the energy loss⁶¹. Adding the two contributions it thus appears that the stopping power of a fully established quark-gluon plasma is probably slightly higher than that of hadronic matter. However, in the vicinity of the deconfinement phase transition (if it exists!) there might be a region where the stopping power of strongly interacting matter *decreases* with growing energy density. One would expect this effect to be particularly pronounced if the phase transition is of second order. The critical opalescence would in this case strongly suppress the emission of gluon radiation from the fast parton. If such an effect could be observed, e.g. by varying the transverse energy produced, it would clearly point toward a strong structural rearrangement in dense hadronic matter, possibly toward a quark-gluon plasma which is dominated by the propagation of collective color modes.

The suppression of J/ψ production, originally proposed by Matsui and Satz⁵⁴, is based on a simple, yet elegant idea: The ground state of ($c\bar{c}$) pair does not exist when the color screening length $\lambda_D = 1/gT$ is less than the bound state radius $\langle r_{J/\psi}^2 \rangle^{1/2}$ (see also Figure 12). Lattice simulations of SU(3) gauge theory^{123,124} show that this condition should be satisfied slightly above the deconfinement temperature ($T/T_c > 1.2$). The screening length appears to be even shorter, when dynamical fermions are included in the lattice simulations¹²⁵. In addition, the D-meson is expected to dissociate in the deconfined phase, lowering the energy threshold ΔE^* for thermal break-up of the J/ψ . Blaschke¹²⁶ has estimated, using the kinetic relation

$$\sigma_{\text{diss}}^{J/\psi} \approx \sigma_0 e^{-\Delta E^*/T}, \quad (77)$$

that the dissociation probability jumps significantly already at T_c , and reaches unity at $T/T_c \simeq 1.2$.

The J/ψ may still survive, if it escapes from the “dangerous” region before the $c\bar{c}$ pair has been spatially separated by more than the size of the bound state, i.e.

more than about 0.5 fm. This may happen, if the quark-gluon plasma cools very fast, or if the J/ψ has sufficiently high transverse momentum¹²⁷: $p_T \geq 3$ GeV/c. The details of J/ψ suppression near T_c are quite complicated and could require a rather long lifetime of the quark-gluon plasma state before becoming clearly visible¹²⁸.

On the other hand, the J/ψ may also be destroyed in a hadronic scenario without phase transition by sufficiently energetic collisions with comoving hadrons¹²⁹, leading to dissociation into a pair of D-mesons. This mechanism has recently been analyzed carefully by Gavin¹³⁰ and by Vogt et al.¹³¹. In addition, the dependence of the suppression factor S on transverse momentum of the J/ψ is explained by a broadening of the transverse momentum distribution of projectile gluons due to prescattering¹³². Drell-Yan data¹³³ of Fermilab experiment E772 indicate that this proceeds like a random walk leading to a broadening $\Delta\langle p_T^2 \rangle$ which grows like $A^{-1/3}$. These effects combine to explain most of the NA38 data. The result of these studies^{130,131} is that the pattern of J/ψ suppression observed in experiment NA38 at CERN¹³⁴ can be understood on the basis of “standard” hadronic interactions, if one assumes comoving hadronic matter at density of at least $1/\text{fm}^3$ and an absorption cross section of the order of 2 mb.

Karsch and Satz have recently analyzed whether this ambiguity persists at RHIC and LHC energies¹³⁵. Assuming that a hadronic phase can be formed at energy densities of $4 - 7.5$ GeV/fm³, they find little difference in $S(p_T)$ in the accessible p_T range. However, they predict a substantial difference in the suppression of the Υ resonance at LHC energies¹³⁶.

Electromagnetic Response Function

Electromagnetic signals for the quark-gluon plasma are in many respects ideal because they probe the earliest and hottest phase of the evolution of the fireball, and are not affected by final state interactions. Their drawbacks are (a) the rather small count rates and (b) the relatively large backgrounds from hadronic decay processes, especially π^0 and η decays. Electromagnetic signals probe the structure of the electromagnetic current response function:

$$\Pi_{\mu\nu}(q^2) = \int d^4x d^4y e^{iq(x-y)} \langle j_\mu(x) j_\nu(y) \rangle. \quad (78)$$

In the hadronic phase, $\Pi_{\mu\nu}(q^2)$ is dominated by the ρ^0 resonance at 770 MeV, whereas perturbative QCD predicts a broad continuous spectrum above twice the thermal quark mass $m_q = gT/\sqrt{6}$. At low $q^2 \ll 100$ MeV collective modes are predicted to exist in both phases. In first approximation the collective quark-gluon plasma excitation, the *plasmino*¹³⁷, has a somewhat higher effective mass than the collective $\pi^+\pi^-$ mode¹³⁸, but its influence is hidden under strong nonresonant effects of soft QCD interactions in the plasma that cause a strong increase at low q^2 (see Figure 29). Unfortunately, these interesting modifications below the mass of the vector mesons will probably be overwhelmed by background from Dalitz pairs¹³⁹.

On the other hand, the production of lepton pairs with large invariant mass in the quark-gluon plasma phase may be sensitive to pre-equilibrium phenomena, e.g. collective plasma oscillations of large amplitude⁷⁸. Such oscillations are known to occur in the framework of the chromo-hydrodynamic model where the collision energy is first stored in a coherent color field which later breaks up into $q\bar{q}$ pairs. The ensuing collective flow could enhance the production of lepton pairs of high invariant mass.

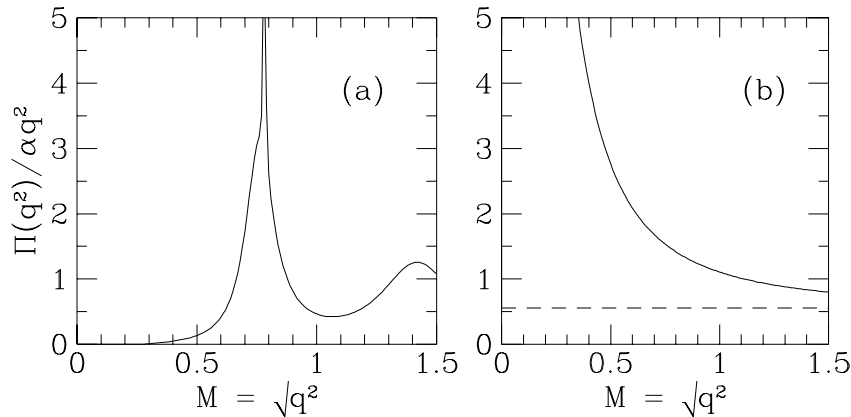


Figure 29. Electromagnetic response function of dense hadronic matter (a) and quark-gluon plasma (b), as function of the invariant mass $\sqrt{q^2}$ of a virtual photon. The hadronic response function is dominated by the neutral vector meson resonances ρ^0, ω , and ϕ . The dashed line in (b) shows the contribution from free quarks, while the solid line includes QCD interactions ($\alpha_s=0.3$). Both cases exhibit collective modes at low q^2 , which are not shown here.

The suggestion by Siemens and Chin¹⁴⁰ that the disappearance of the ρ -meson peak in the lepton pair mass spectrum would signal the deconfinement transition has recently been revived¹⁴¹. The basic idea is to utilize the fact that the quark-gluon plasma phase should exhibit the higher temperature than the hadronic phase, and therefore lepton pairs from the quark-gluon plasma should dominate at high p_T over those originating from hadronic processes. Unfortunately, the reasoning probably breaks down when one allows for collective transverse flow. Because of its larger mass, the ρ -meson spectrum is much more sensitive to the presence of flow than the quark spectrum in the quark-gluon plasma phase¹⁴².

Nonetheless, the lepton pairs from ρ -meson decay can be a very useful tool for probing the hadronic phase of the fireball. Heinz and Lee¹⁴³ have pointed out that the ρ -peak is expected to grow strongly relative to the ω - and ϕ - peaks in the electron pair mass spectrum, if the fireball lives substantially longer than 2 fm/c. This occurs because of the short average lifetime of the ρ (1.3 fm/c), so that several generations of thermal ρ^0 -mesons would contribute to the spectrum. In the limit of a very long-lived fireball the ratio of lepton pairs from ρ^0 - and ω - decays would approach the ratio of their leptonic decay widths (11:1). The ρ/ω -ration can therefore serve as a fast “clock” for the fireball lifetime.

The widths and positions of the ρ , ω , and ϕ peaks should also be sensitive to medium induced changes of the hadronic mass spectrum, especially to precursor phenomena associated with chiral symmetry restoration. This has been studied extensively¹⁴⁴. The general conclusion, however, is that these modifications are probably small except in the immediate vicinity of the phase transition. Changes are predicted to occur sooner, if the hadronic phase contains an appreciable net baryon density. E.g. a change in the K-meson mass could be detected via the induced change in the width of the ϕ -meson¹⁴⁵.

Direct photons, the second electromagnetic probe of dense matter, must face the formidable background from π^0 and η - decays. Whether these decays can be reconstructed and subtracted with sufficient reliability remains questionable, despite the remarkable achievements in this respect by experiment WA80 at CERN¹⁴⁶. But even if it were possible, it is not clear what direct photons would tell. A new calculation by photon emission from hadronic matter and quark-gluon plasma at the same

temperature ($T=200$ MeV) by Kapusta, Lichard and Seibert¹⁴⁷ has yielded virtually identical results for the two scenarios. This is by no means trivial, because the fireball is optically thin. The result is a consequence of the presence of thermal ρ -mesons and only occurs when the process $\pi\rho \rightarrow \pi\gamma$ is taken into account.

Altogether, the prospects for an unambiguous quark-gluon plasma signal from the electromagnetic sector are doubtful. Moreover, the count rates predicted at the future heavy ion colliders (RHIC and LHC) are quite small. The situation is reviewed in more detail by V. Ruuskanen¹⁴⁸. However, one should recall that electromagnetic probes are most sensitive to the earliest phase of a nuclear collision⁹⁰, and thus might prove to be a valuable tool for the detection of pre-equilibrium phenomena⁹³, even if they should eventually turn out not to be good probes of the thermal quark-gluon plasma.

Exotica

It would be nice if the formation of quark-gluon plasma would be associated with the appearance of completely novel phenomena: there would be no ambiguity in such signatures. Indeed one should remember that the proposal to look for quark-gluon plasma in nuclear collisions¹⁴⁹ was originally derived from the apparent existence of unexplained phenomena observed in cosmic ray interaction, such as the famous “Centauro” events. The most probable exotic objects that might be formed from quark-gluon plasma are *strangelets*^{46–48}. As explained earlier, this name describes metastable objects with baryon number $A \geq 2$ that contain several strange quarks. The simplest such object is the strangeness $S = -2$ dibaryon, the H -particle, which is predicted to be metastable in the original MIT bag model¹⁵¹ and might be produced in relativistic nuclear collisions¹⁵². Experiments⁴⁹ searching for strangelets produced in relativistic heavy ion reactions are in progress at BNL, and in preparation at CERN.

Recently there has been speculation about the possible formation of locally “dis-oriented” chiral vacua in relativistic nuclear collisions¹⁵³. Such states would decay into a large number of pions, possibly with a strong isospin imbalance as observed in the Centauro events. They might be produced by some not well understood collective emission process, or by spontaneous symmetry breaking when the dense hadronic system returns from the chirally restored phase.

CONCLUSIONS

It is appropriate to conclude this review of quark-gluon plasma physics by emphasizing the positive aspects. Many of the proposed quark-gluon plasma signals have actually been observed already in the present experiments: J/ψ suppression; enhanced production of strange hadrons, most notably of strange antibaryons; increase in transverse momenta of emitted particles. None of these results has been demonstrated to be an unambiguous signal of the quark-gluon plasma, so far. However, one should bear in mind that the experiments were all performed with systems that were too small (Si and S are hardly “heavy” nuclei) and at energies too low to expect the formation of a full-fledged, sufficiently long-lived quark-gluon plasma state. In view of this, the experimental results are encouraging.

On the theoretical side, a better understanding of what we really mean by a “quark-gluon plasma signature” is required¹⁵⁴. In practical terms, we need a consistent formulation of what precisely is measured by J/ψ -suppressing and antihyperon enhancement. How do these signatures depend on the color response function or the

quark correlation function $\langle q\bar{q} \rangle$ in the medium? Finally, we need to understand how pre-equilibrium processes influence predictions for the proposed signatures. These are difficult questions but, as I have tried to show, our understanding of the physics of the quark-gluon plasma has progressed to the point where these problems can be seriously addressed.

Acknowledgements

I want to thank the organizers of the NATO-Advanced Study Institute at Il Ciocco, especially H. Gutbrod and J. Rafelski for providing opportunities of intense discussion that helped clarify several points contained in these lecture notes. I am deeply indebted to T. Biró, K. Geiger, C. Gong, P. Lévai, J. Rau, M. Thoma, A. Trayanov, and X. N. Wang, who helped develop many of the ideas presented here. I thank W. A. Zajc for pointing out several errors. This work was partially supported by the U.S. DOE (Grant DE-FG05-90ER40592), NCSC and NATO.

REFERENCES

1. B. Müller, *The Physics of the Quark-Gluon Plasma*, Lecture Notes in Physics, Vol. 225 (Springer-Verlag, Berlin-Heidelberg 1985).
2. L. McLerran, *Rev. Mod. Phys.* **58**, 1021 (1986).
3. *Quark-Gluon Plasma*, edited by R. C. Hwa (World Scientific, Singapore, 1991).
4. For a recent review of cosmological implications of the quark-gluon phase transition, see:
K. A. Olive, *Science* **251**, 1194 (1991) and references therein.
5. See e.g.: E. W. Kolb and M. S. Turner, *The Early Universe* (Addison-Wesley, Redwood City, 1990), Chap. 3.5.
6. A. Guth, *Phys. Rev.* **D23**, 347 (1981).
7. L. F. Abbot and S. Y. Pi, *Inflationary Cosmology*, Reprint volume (World Scientific, Singapore, 1986).
8. J. Ellis, J. I. Kapusta, and K. A. Olive, *Nucl. Phys.* **B348**, 345 (1991).
9. N. K. Glendenning, *Phys. Rev. Lett.* **63**, 2629 (1989).
10. R. Hagedorn, in: *Quark Matter '84*, ed. by K. Kajantie, *Lecture Notes in Physics* Vol. 221, p. 53 (Springer-Verlag, Berlin-Heidelberg, 1985).
11. J. D. Walecka, *Phys. Lett.* **59B**, 109 (1975); J. Theis, et al., *Phys. Rev.* **D28**, 2286 (1983).
12. J. Gasser and H. Leutwyler, *Phys. Lett.* **188B**, 477 (1987).
13. P. Carruthers, *Collective Phenomena*, **1**, 147 (1973).
14. J. C. Collins and M. Perry, *Phys. Rev. Lett.* **34**, 1353 (1975).
15. G. Baym and S. A. Chin, *Phys. Lett.* **62B**, 241 (1976); S. A. Chin, *Phys. Lett.* **78B**, 552 (1978).
16. B. Friedman and L. McLerran, *Phys. Rev.* **D17**, 1109 (1978); L. D. McLerran, *Phys. Rev.* **D24**, 450 (1981).
17. E. V. Shuryak, *Phys. Rep.* **61**, 71 (1980).
18. R. Hagedorn, *Suppl Nuovo Cimento* **3**, 147 (1965).

19. See e.g.: M. B. Green, J. H. Schwarz, and E. Witten, *Superstring Theory*, Vol. 1, chap. 2.3.5.
(Cambridge University Press, Cambridge, 1987).
20. J. Kapusta, *Phys. Rev.* **D23**, 2444 (1981).
21. K. Sailer, B. Müller, and W. Greiner, *Int. J. Mod. Phys.* **A4**, 437 (1989).
22. N. Cabibbo and G. Parisi, *Phys. Lett.* **59B**, 67 (1975).
23. R. Hagedorn and J. Rafelski, *Phys. Lett.* **97B**, 136 (1980).
24. E. Shuryak, *Nucl. Phys.* **A533**, 761 (1991); E. Shuryak and V. Thorsson, *Nucl. Phys.* **A536**, 739 (1992).
25. C. Gong, *J. Phys.* **B18**, L123 (1992).
26. T. Abbott, et al. [E-802 Collaboration], *Phys. Rev. Lett.* **64**, 847 (1990).
27. G. E. Brown and M. Rho, *Phys. Rev. Lett.* **66**, 2720 (1991).
28. See e.g.: L. J. Reinders, H. R. Rubinstein, and S. Yazaki, *Phys. Rep.* **127**, 1 (1985).
29. R. J. Furnstahl, T. Hatsuda, and S. H. Lee, *Phys. Rev.* **D42**, 1744 (1990).
30. G. Adami, T. Matsuda, and I. Zahed, *Phys. Rev.* **D43**, 921 (1991).
31. T. D. Cohen, R. J. Furnstahl, and D. K. Griegel, *Phys. Rev.* **C45**, 1881 (1992).
32. A. X. El-Khadra, G. Hockney, A. S. Kronfeld, and P. B. Mackenzie, *Phys. Rev. Lett.* **69**, 729 (1992).
33. M. Creutz, *Quarks, Gluons and Lattices* (Cambridge University Press, Cambridge, 1983).
34. F. R. Brown, et al., *Phys. Rev. Lett.* **65**, 2491 (1990); see also the lecture by F. Karsch at this School.
35. See e.g. the lecture by L. P. Csernai at this School.
36. E. Farhi and R. L. Jaffe, *Phys. Rev.* **D30**, 2379 (1984); I. Mardor and B. Svetitsky, *Phys. Rev.* **D44**, 878 (1991).
37. S. Huang, J. Potvin, C. Rebbi, and S. Sanielevici, *Phys. Rev.* **D42**, 2864 (1990); **D43**, 2056E (1991); K. Kajantie, L. Karkkainen, and K. Rummukainen, *Nucl. Phys.* **B357**, 693 (1991).
38. L. P. Csernai and J. I. Kapusta, preprint TPI-MINN-92-10-T, University of Minnesota, March 1991; *Phys. Rev. Lett.* **69**, 737 (1992).
39. G. Lana and B. Svetitsky, *Phys. Lett.* **B285**, 251 (1992).
40. J. Potvin, Talk at the Workshop on QCD Vacuum Structure, Paris, June 1992 (to be published).
41. E. Witten, *Phys. Rev.* **D30**, 272 (1984).
42. J. H. Applegate and C. J. Hogan, *Phys. Rev.* **D31**, 3037 (1985); **D34**, 1938 (1986); C. Alcock, G. M. Fuller, and G. J. Mathews, *Astrophys. J.* **320**, 439 (1987).
43. M. Kurki-Suonio and R. Matzner, *Phys. Rev.* **D39**, 1046 (1989); *Phys. Rev.* **D42**, 1047 (1990); H. Kurki-Suonio, et al., *Astrophys. J.* **353**, 406 (1990).
44. G. J. Mathews, B. Meyer, C. R. Alcock, and G. M. Fuller, *Astrophys. J.* **358**, 406 (1990).
45. A. Bodmer, *Phys. Rev.* **D4**, 1601 (1971); S. Chin and A. Kerman, *Phys. Rev. Lett.* **43**, 1291

- (1978); E. Farhi and R. Jaffe, *Phys. Rev.* **D30**, 2379 (1984).
46. H. Liu and G. Shaw, *Phys. Rev.* **D30**, 1137 (1984).
 47. C. Greiner, P. Koch, and H. Stöcker, *Phys. Rev. Lett.* **58**, 1825 (1987); *Phys. Rev.* **D38**, 2797 (1988).
 48. C. Greiner, D. Rischke, H. Stöcker, and P. Koch, *Z. Phys.* **C38**, 283 (1988); C. Greiner and H. Stöcker, *Phys. Rev.* **D44**, 3517 (1991); G. Shaw, G. Benford, and D. Silverman, *Phys. Lett.* **169B**, 275 (1986).
 49. Brookhaven Experiments E814 (J. Barrette, et al., *Phys. Lett.* **B252**, 550 (1990)), E864 (J. Sandweis, et al.); E878 (H. J. Crawford, et al.); CERN-Experimental Proposal SPSLC/ P-268 (K. Pretzl, et al.).
 50. G. Shaw, M. Shin, R. Dalitz, and M. Desai, *Nature* **337**, 436 (1989); M. S. Desai and G. Shaw, Technological Implications of Strange Quark Matter, to appear in *Nucl. Phys. B*.
 51. J. Kapusta, *Nucl. Phys.* **B148**, 461 (1979).
 52. V P. Silin, *Sov. Phys. JETP* **11**, 1136 (1960); V. V. Klimov, *Sov. Phys. JETP* **55**, 199 (1982); H. A. Weldon, *Phys. Rev.* **D26**, 1394 (1982).
 53. A. Billoire, G. Lazarides, and Q. Shafi, *Phys. Lett.* **103B**, 450 (1981); T. A. DeGrand and D. Toussaint, *Phys. Rev.* **D25**, 526 (1982). These authors find a coefficient $C = 0.27 \pm 0.03$ for SU(2) gauge theory.
 54. T. Matsui and H. Satz, *Phys. Lett* **178B**, 416 (1986).
 55. R. D. Pisarski, *Phys. Rev. Lett.* **63**, 1129 (1989); E. Braaten and R. D. Pisarski ; *Phys. Rev.* **D42**, 2156 (1990).
 56. A. Ukawa, *Nucl. Phys.* **A498**, 227c (1989).
 57. T. Biró, P. Lévai, and B. Müller, *Phys. Rev.* **D42**, 3078 (1990).
 58. M. H. Thoma, *Phys. Lett.* **B269**, 144 (1991); G. Baym, H. Monien, C. J. Pethick, and D. G. Ravenhall, *Phys. Rev. Lett.* **64**, 1867 (1990).
 59. E. Shuryak, *Phys. Rev. Lett.* **68**, 3270 (1992).
 60. A. B. Migdal, *Sov. Phys. JETP* **5**, 527 (1957).
 61. A. H. Sørensen, *Z. Phys.* **C53**, 595 (1992); M. Gyulassy and X. N. Wang, to be published.
 62. M. H. Thoma and M. Gyulassy, *Nucl. Phys.* **B351**, 491 (1991); E. Braaten and M. H. Thoma, *Phys. Rev.* **D44**, R2525 (1991).
 63. S. Mrówczyński, *Phys. Lett.* **B269**, 383 (1991).
 64. N. S. Krylov, *Works on the Foundation of Statistical Physics* (Princeton University Press, Princeton, 1979); A. N. Kolmogorov, *Dokl. Akad. Nauk SSSR* **119**, 861 (1958) and **124**, 754 (1959); Ya. G. Sinai, *Dokl. Akad. Nauk SSSR* **124**, 768 (1959) and **125**, 1200 (1959). See also: G. M. Zaslavsky, *Chaos in Dynamic Systems* (Harwood, Chur, 1985).
 65. Gun He, *Phys. Lett.* **A149**, 95 (1990).
 66. S. G. Matinyan, G. K. Savvidy, and N. G. Ter-Arutyunyan-Savvidy, *Sov. Phys. JETP* **53**, 421

- (1981); *JETP Lett.* **34**, 590 (1981); See also: C. Gong, B. Müller, and A. Trayanov, preprint DUKE-TH-92-34 and references therein.
67. B. Müller and A. Trayanov, *Phys. Rev. Lett.* **68**, 3387 (1992).
 68. C. Gong, preprint DUKE-TH-92-41.
 69. B. Anderson, G. Gustafson, G. Ingelman, and T. Sjöstrand, *Phys. Rep.* **97**, 31 (1983).
 70. B. Nilsson-Almquist and E. Stenlund, *Comp. Phys. Comm.* **43**, 387 (1987).
 71. M. Gyulassy, preprint CERN-TH-4784 (1987, unpublished).
 72. T. Csörgő, J. Zimányi, J. Bondorf, and H. Heiselberg, *Phys. Lett.* **B222**, 115 (1989).
 73. K. Werner, *Z. Phys.* **C42**, 85 (1989).
 74. N. S. Amelin, K. K. Gudima, and V. D. Toneev, *Yad. Fiz.* **51**, 512 (1990).
 75. M. Sorge, H. Stöcker, and W. Greiner, *Nucl. Phys.* **A498**, 567c (1989); *Ann. Phys.* **192**, 266 (1989).
 76. T. S. Biró, H. B. Nielsen, and J. Knoll, *Nucl. Phys.* **B245**, 449 (1984).
 77. A. Białas and W. Czyż, *Phys. Rev.* **D31**, 198 (1985); *Nucl. Phys.* **B267**, 242 (1986); S. Kagiya, A. Nakamura, and A. Minaka, *Prog. Theor. Phys.* **75**, 319 (1986).
 78. K. Kajantie and T. Matsui, *Phys. Lett.* **B164**, 373 (1985); G. Gatoff, A. K. Kerman, and T. Matsui, *Phys. Rev.* **D36**, 114 (1986); M. Asakawa and T. Matsui, *Phys. Rev.* **D43**, 2871 (1991); G. Gatoff, preprint ORNL/CCIP/91/24, Oak Ridge, 1991.
 79. D. Boal, *Phys. Rev.* **C33**, 2206 (1986).
 80. R. C. Hwa and K. Kajantie, *Phys. Rev. Lett.* **56**, 696 (1986).
 81. J. P. Blaizot and A. H. Mueller, *Nucl. Phys.* **B289**, 847 (1987).
 82. F. Niedermayer, *Phys. Rev.* **D34**, 3494 (1986).
 83. P. Lévai and B. Müller, preprint DUKE-TH-90-10.
 84. J. D. Bjorken, *Phys. Rev.* **D27**, 140 (1983).
 85. K. Geiger and B. Müller, *Nucl. Phys.* **B369**, 600 (1992); see also lecture by K. Geiger at this School.
 86. (a) T. Sjöstrand and M. van Zijl, *Phys. Rev.* **D36**, 2019 (1987);
(b) N. Abou-El-Naga, K. Geiger, and B. Müller, *J. Phys.* **G18**, 797 (1992).
 87. X. N. Wang and M. Gyulassy, *Phys. Rev.* **D44**, 3501 (1991).
 88. T. Biró, B. Müller, and X. N. Wang, *Phys. Lett.* **B283**, 171 (1992).
 89. A recent calculation⁹⁰ of lepton-pair production from the quark-gluon plasma assumes that quarks come into thermal equilibrium with $T = 900$ MeV at LHC energy. Our arguments indicate that, although this value of T may adequately describe the quark spectrum, the phase space density of quarks will be far below thermal, strongly reducing the lepton-pair yield.
 90. J. Kapusta, L. McLerran, and D. K. Srivastava, *Phys. Lett.* **B283**, 145 (1992).
 91. K. Geiger, preprints UMSI 92/113, 92/174 and 92/175, University of Minnesota (1992).
 92. B. Müller and X. N. Wang, *Phys. Rev. Lett.* **68**, 2437 (1992).
 93. I. Kawrakow and J. Ranft, preprint UL-HEP-92-08, Leipzig (1992); B. Kämpfer and O. P. Pavlenko, *Phys. Lett.* **B289**, 127 (1992).

94. J. Cleymans and R. Philippe, *Z. Phys.* **C22**, 271 (1984); J. Cleymans and C. Vanderzande, *Phys. Lett.* **147B**, 186 (1984).
95. J.P. Blaizot and J.Y. Ollitrault, in: Ref. 3, p. 393; see also: H. von Gersdorff, L. McLerran, M. Kataja, and P. V. Ruuskanen, *Phys Rev.* **D34**, 794 (1986); M. Kataja, P. V. Ruuskanen, L. McLerran, and H. von Gersdorff, *Phys Rev.* **D34**, 794 (1986).
96. K. Kajantie and L. McLerran, *Ann. Rev. Nucl. Sci.* **37**, 293 (1987).
97. *QGP Signatures*, edited by V. Bernard, et al. (Editions Frontières, Paris, 1990).
98. L. van Hove, *Phys. Lett.* **118B**, 138 (1982); *Z. Phys.* **C21**, 93 (1983).
99. H. von Gersdorff, *Nucl. Phys.* **A461**, 251c (1987).
100. T. Alexopoulos. et al., *Phys. Rev. Lett.* **64**, 991 (1990); see also L. Gutay's lecture at this School.
101. P. Lévai and B. Müller, *Phys. Rev. Lett.* **67**, 1519 (1991).
102. Such data are now becoming available [A. Goshaw, Duke University, private communication.]
103. X. N. Wang and M. Gyulassy, *Phys. Lett.* **B282**, 466 (1992).
104. See e.g. the lecture by W. Zajc at this School.
105. M. Lahanas, et al. [NA35 collaboration], *Nucl. Phys.* **A525**, 327c (1991).
106. J. Rafelski, *Phys. Rep.* **88**, 331 (1982).
107. J. Rafelski and B. Müller, *Phys. Rev. Lett.* **48**, 1066 (1982); **56**, 2334E (1986).
108. P. Koch, B. Müller, and J. Rafelski, *Phys. Rep.* **142**, 167 (1986).
109. C. M. Ko, et al., *Phys. Rev. Lett.* **66**, 2577 (1991).
110. T. Abbott, et al. [E-802 collaboration], *Phys. Lett.* **B197**, 285 (1987); *Phys. Rev. Lett.* **64**, 847 (1990); S. E. Eiseman, et al. [E-810 collaboration]. *Phys. Lett.* **B248**, 254 (1990); J. Bartke, et al. [NA35 collaboration], *Z. Phys.* **C48**, 191 (1990); H. van Hecke, et al. [HELIOS collaboration], *Nucl. Phys.* **A525**, 227c (1991); S. Abatzis, et al. [WA85 collaboration], *Phys. Lett.* **B270**, 123 (1991); E. Andersen, et al. [NA36 collaboration], submitted to *Phys. Lett. B*; For reviews see: O. Hansen, *Comments Nucl. Part. Phys.* **20**, 1 (1991); G. Odyniec, preprint LBL-29996, published in ref. 97.
111. R. Mattiello, H. Sorge, H. Stöcker, and W. Greiner, *Phys. Rev. Lett.* **63**, 1459 (1989).
112. N. N. Nikolaev, *Z. Phys.* **C44**, 645 (1989).
113. E. Quercigh, Lecture at this School.
114. J. Rafelski, *Phys. Lett.* **262B**, 333 (1991), and lecture at this School.
115. J. Letessier, A. Tounsi, and J. Rafelski, preprint PAR/LPTHE/92-23, Paris (1992).
116. N. J. Davison, H. G. Miller, R. M. Quick, and J. Cleymans, *Phys. Lett.* **255B**, 105 (1991).
117. J. Aichelin and K. Werner, preprint HD-TVP-91-15 and HD-TVP-91-18, Heidelberg (1991).
118. H. Sorge, M. Berenguer, H. Stöcker, and W. Greiner, preprint LA-UR-92-1078; see also the lecture by M. Sorge at this School.
119. J. P. Guillaud, et al. [NA38 collaboration], *Nucl. Phys.* **A525**, 449c (1991).
120. P. Koch and U. Heinz, *Nucl. Phys.* **A525**, 293c (1991); see also lecture by P. Koch at this School.
121. J. D. Bjorken, Fermilab pub. 82/59, Batavia (unpublished).

122. Y. Koike and T. Matsui, preprint, U. of MD PP #91-223, Maryland (1991).
123. T. A. DeGrand and C. E. DeTar, *Phys. Rev.* **D34**, 2469 (1986); K. Kanaya and H. Satz, *Phys. Rev.* **D34**, 3193 (1986).
124. F. Karsch, *Z. Phys.* **C38**, 147 (1988).
125. F. Karsch and H. W. Wyld, *Phys. Lett.* **213B**, 505 (1988).
126. D. Blaschke, *Nucl. Phys.* **A525**, 269c (1991).
127. F. Karsch and R. Petronzio, *Phys. Lett.* **212B**, 255 (1988); J. P. Blaizot and J. Y. Ollitraut, *Phys. Lett.* **199B**, 499 (1987).
128. S. Hioki, T. Kanki, and O. Miyamura, *Prog. Theor. Phys.* **84**, 317 (1990); **85**, 603 (1991).
129. S. Gavin, M. Gyulassy, and A. Jackson, *Phys. Lett.* **207B**, 257 (1988).
130. S. Gavin, R. Vogt, *Nucl. Phys.* **B345**, 104 (1990); S. Gavin, preprint HU-TFT-91-33, Helsinki (1991).
131. R. Vogt, S. J. Brodsky, and P. Hoyer, *Nucl. Phys.* **B360**, 67 (1991).
132. J. Blaizot and J. Y. Ollitraut, *Phys. Lett.* **217B**, 392 (1989).
133. J. M. Moss, et al. [E-772 collaboration], *Nucl. Phys.* **A525**, 285c (1991).
134. A. Guichard, et al. [NA38 collaboration], *Nucl. Phys.* **A525**, 467c (1991).
135. F. Karsch and H. Satz, preprint CERN-TH-5900/90, *Z. Phys. C* (in press).
136. Possibly because their quark-gluon plasma scenario is oversimplified. Also the analysis of the hadronic scenario is based on unrealistically high energy densities in a pure pion gas.
137. H. A. Weldon, *Phys. Rev. Lett.* **66**, 283 (1991).
138. C. Gale and J. Kapusta, *Phys. Rev.* **D43**, 3080 (1991).
139. E. Braaten, R. D. Pisarski, and T. C. Yuan, *Phys. Rev. Lett.* **64**, 2242 (1990).
140. P. J. Siemens and S. A. Chin, *Phys. Rev. Lett.* **55** 1266 (1985).
141. D. Seibert, *Phys. Rev. Lett.* **68**, 1476 (1992).
142. M. Kataja, P. V. Ruuskanen, J. Letessier, and A. Tounsi, preprint, University of Jyväskylä and LPTHE, Univ. Paris VII (1991).
143. U. Heinz and K. S. Lee, *Phys. Lett.* **259B**, 162 (1991).
144. H. W. Barz, G. Bertsch, B. L. Friman, H. Schulz and S. Boggs, *Phys. Lett.* **265B**, 219 (1991); C. Chanfray and P. Schuck, preprint, Grenoble 1991; Z. Aouissat, G. Chanfray, P. Schuck, and G. Welke, preprint, Grenoble 1991; C. M. Ko, P. Lévai and W. J. Qin, preprint, Texas A&M University 1991.
145. D. Lissauer and E. V. Shuryak, *Phys. Lett.* **253B**, 15 (1991); P. Z. Bi and J. Rafelski, *Phys. Lett.* **262B**, 485 (1991).
146. R. Albrecht, et al. [WA80 collaboration], *Z. Phys.* **C51**, 1 (1991).
147. J. Kapusta, P. Lichard, and D. Seibert, *Phys. Rev.* **D44**, 2774 (1991).
148. P. V. Ruuskanen, *Nucl. Phys.* **A525**, 255c (1991); see also the lecture by P. V. Ruuskanen at this School.
149. S. A. Chin and A. K. Kerman, *Phys. Rev. Lett.* **43**, 1292 (1979).
150. M. Tamada, *Nuovo Cim.* **41B**, 245 (1977).
151. R. L. Jaffe, *Phys. Rev. Lett.* **38**, 195 (1977); **38**, 1617E (1977).
152. C. B. Dover, P. Koch and M. May, *Phys. Rev.* **C40**, 115 (1989).

153. A. A. Anselm and M. G. Ryskin, *Phys. Lett.* **B266**, 482 (1991); J. D. Bjorken, preprints
SLAC-PUB-5545 and -5673, Stanford (1991); J. P. Blaizot and A. Krzywicki, preprint LPTHE Orsay 92/11.
154. B. Müller and S. Schramm, *Phys. Rev.* **C43**, 2791 (1991); B. Müller, *Nucl. Phys.* **A544**, 95c
(1992).